

# Aneuploidy can be an evolutionary detour on the path to adaptation

Ilia Kohanovski<sup>a,b,1</sup>, Martin Pontz<sup>a,1</sup>, Orna Dahan<sup>c</sup>, Yitzhak Pilpel<sup>c</sup>, Avihu H.  
Yona<sup>d</sup>, and Yoav Ram<sup>a,\*</sup>

<sup>a</sup>School of Zoology, Faculty of Life Sciences, Tel Aviv University, Tel Aviv, Israel

<sup>b</sup>School of Computer Science, Reichman University, Herzliya, Israel

<sup>c</sup>Department of Molecular Genetics, Weizmann Institute of Science, Rehovot, Israel

<sup>d</sup>Institute of Biochemistry, Food Science and Nutrition, Robert H. Smith Faculty of Agriculture, Food and Environment, The Hebrew University of Jerusalem, Israel

<sup>1</sup>These authors contributed equally to this work

\*Corresponding author: yoav@yoavram.com

November 23, 2023

Classifications. Biological Sciences: Evolution, Genetics, Microbiology, Population Biology.

Keywords: whole-chromosome duplication, evolutionary model, adaptive evolution

## Abstract

16 Aneuploidy is common in eukaryotes, often leading to decreased fitness. However, evidence  
from fungi and human tumour cells suggests that specific aneuploidies can be beneficial under  
18 stressful conditions and facilitate adaptation. In a previous evolutionary experiment with yeast,  
populations evolving under heat stress became aneuploid, only to later revert to euploidy after  
20 beneficial mutations accumulated. It was therefore suggested that aneuploidy is a "stepping stone"  
on the path to adaptation. Here, we test this hypothesis. We use Bayesian inference to fit an  
22 evolutionary model with both aneuploidy and mutation the experimental results. We then predict  
the genotype frequency dynamics during the experiment, demonstrating that most of the evolved  
24 euploid population likely did not descend from aneuploid cells, but rather from the euploid wildtype  
population. Our model shows how the beneficial mutation supply—the product of population size  
26 and beneficial mutation rate—determines the evolutionary dynamics: with low supply, much of  
the evolved population descends from aneuploid cells; but with high supply, beneficial mutations  
28 are generated fast enough to outcompete aneuploidy due to its inherent fitness cost. Our results  
suggest that despite its potential fitness benefits under stress, aneuploidy can be an evolutionary  
30 "detour" rather than a "stepping stone": it can delay, rather than facilitate, the adaptation of the  
population, and cells that become aneuploid may leave less descendants compared to cells that  
32 remain diploid.

# Introduction

34 Aneuploidy is an imbalance in the number of chromosomes in the cell: an incorrect karyotype.  
Evidence suggests aneuploidy is very common in eukaryotes, e.g. animals<sup>49,38,2</sup>, and fungi<sup>41,73,45,62</sup>.  
36 Aneuploidy has been implicated in cancer formation, progression, and drug resistance<sup>4,51,49,48,23,34</sup>.  
It is also common in protozoan pathogens of the *Leishmania* genus, a major global health concern<sup>36</sup>,  
38 and contributes to the emergence of drug resistance<sup>52</sup> and virulence<sup>37</sup> in fungal pathogens, which  
are under-studied<sup>47</sup>, despite infecting a billion people per year, causing significant morbidity in >150  
40 million and death in >1.5 million people per year<sup>52,47</sup>.

Experiments with human and mouse embryos found that most germ-line aneuploidies are lethal. An-  
42 uploidies are also associated with developmental defects and lethality in other multicellular organ-  
isms<sup>55</sup>. For example, aneuploid mouse embryonic cells grow slower than euploid cells<sup>67</sup>. Similarly,  
44 in unicellular eukaryotes growing in benign conditions, aneuploidy usually leads to slower growth and  
decreased overall fitness, in part due to proteotoxic stress due to increased expression, gene dosage  
46 imbalance, and hypo-osmotic-like stress<sup>39,65,41,55,50,27,72,66,68,46</sup>.

However, aneuploidy can be beneficial under stressful conditions due to the wide range of phenotypes  
48 it can produce, some of which are advantageous<sup>41,68</sup>. Indeed, in a survey of 1,011 yeast strains,  
aneuploidy has been detected in about 19%<sup>42</sup>. Thus, aneuploidy can lead to rapid adaptation in  
50 unicellular eukaryotes<sup>17,64,21,44</sup>, as well as to rapid growth of somatic tumour cells<sup>51,57</sup>. For example,  
aneuploidy in *Saccharomyces cerevisiae* facilitates adaptation to a variety of stressful conditions like  
52 heat and pH<sup>70</sup>, copper<sup>8,17</sup>, salt<sup>11,46</sup>, and nutrient limitation<sup>12,19,1</sup>, with similar results in *Candida*  
*albicans*<sup>68</sup>. Importantly, aneuploidy can also lead to drug resistance in pathogenic fungi such as  
54 *C. albicans*<sup>54,53,16</sup> and *Cryptococcus neoformans*<sup>58</sup>, which cause candidiasis and meningoencephalitis,  
respectively. Although we focus here on aneuploidy, a similar phenomena of adaptation via gene  
56 duplication or amplification has been observed in yeast<sup>33</sup>, bacteria<sup>60</sup>, and DNA viruses<sup>13</sup>.

Yona et al.<sup>70</sup> demonstrated experimentally the importance of aneuploidy in adaptive evolution. They  
58 evolved populations of *S. cerevisiae* under strong heat stress. The populations adapted to the heat stress  
within 450 generations, and this adaptation was determined to be due a duplication of Chromosome  
60 III. Later on, after more than 1,500 generations, the populations reverted back to an euploid state, while  
remaining adapted to the heat stress. Aneuploidy was therefore suggested to be a *transient adaptive*  
62 *solution*, because it can rapidly appear and fixate in the population under stressful conditions, and can  
then be rapidly lost when the cost of aneuploidy outweighs its benefit—after the stress is removed,  
64 or after "refined" beneficial mutations appear and fixate<sup>70</sup>. Furthermore, it has been suggested that

aneuploidy is an evolutionary "stepping stone" that facilitates future adaptation by genetic mutations,  
66 which require more time to evolve<sup>70,69</sup>.

Here, we test the hypothesis that aneuploidy is a an *evolutionary stepping stone* that facilitates  
68 adaptive evolution by genetic mutations Yona et al.<sup>69</sup>. We develop an evolutionary genetic model and  
fit it to the experimental results of Yona et al.<sup>70</sup> to predict the genotype frequency dynamics in the  
70 experimental populations, thereby estimating the frequency of evolved euploid cells that descended  
from aneuploid cells. Our results show that although aneuploidy reached high frequencies in the  
72 experimental populations, the majority of cells in the evolved euploid population likely did not  
descend from aneuploid cells, but rather directly from wild-type euploid cells. These suggests that at  
74 the lineage level, aneuploidy may be an evolutionary detour, rather than a stepping stone, on the path  
to adaptation.

## 76 Results

In the heat-stress experiment of Yona et al.<sup>70</sup>, four populations of *S. cerevisiae* evolved under 39 °C.  
78 Aneuploidy fixed in all four experimental repetitions in the first 450 generations. Two of the repetitions,  
marked *H2* and *H4*, carried no large-scale duplications other than a Chromosome III trisomy. These  
80 two repetitions continued to evolve under the same conditions, wherein aneuploidy was eliminated by  
generation 1,700 and 2,350 in *H4* and *H2*, respectively.

82 **Evolutionary genetic model.** To explore the dynamics during the evolutionary experiments, we  
developed an evolutionary genetic model, fitted the model to empirical data, and used it to predict the  
84 genotype frequency dynamics, or specifically, the fraction of the evolved euploid population descended  
from aneuploid cells.

86 The model includes the effects of natural selection, genetic drift, aneuploidy, and mutation, and follows  
a population of cells characterized by their genotype: euploid wild-type,  $2n$ , is the ancestral diploid  
88 genotype; euploid mutant,  $2n^*$ , has a diploid karyotype and a single beneficial mutation; aneuploid  
wild-type,  $2n+1$ , has an extra chromosome due to a chromosome duplication event; and aneuploid  
90 mutant,  $2n+1^*$ , has and extra chromosome (like  $2n+1$ ) and a beneficial mutation (like  $2n^*$ ). Fitness  
values of the different genotypes are denoted by  $w_{2n}$ ,  $w_{2n^*}$ ,  $w_{2n+1}$ , and  $w_{2n+1^*}$ , and the rate of mutation  
92 and aneuploidy are denoted by  $\mu$  and  $\delta$ , respectively. See Figure 1 for an illustration of the model.

We fitted this model to the experimental results<sup>70</sup> – time for fixation (>95%) and for loss (<5%) of  
94 aneuploidy – using approximate Bayesian computation with sequential Monte Carlo (ABC-SMC)<sup>59</sup>,

thereby inferring the model parameters: rates aneuploidy and mutation and the fitness of all genotypes.  
 96 We then sampled posterior predictions for the genotype frequency dynamics using the estimated  
 parameter values and compared different versions of the model to test additional hypotheses about the  
 98 evolutionary process.

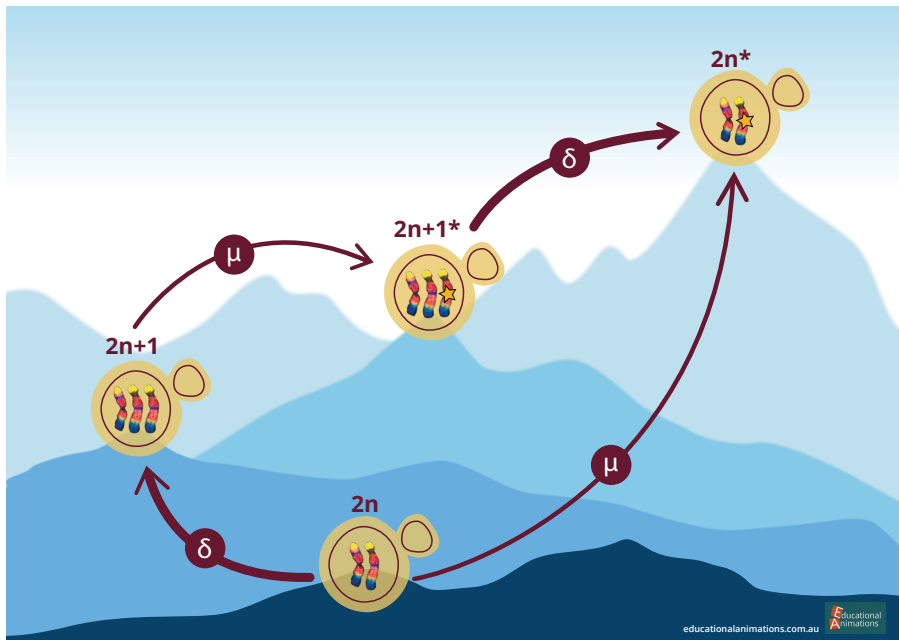


**Figure 1: Model Illustration.** There are four genotypes in our model: euploid wild-type,  $2n$ ; euploid mutant,  $2n^*$ ; aneuploid wild-type,  $2n+1$ ; and aneuploid mutant,  $2n+1^*$ . Overall there are two possible trajectories from  $2n$  to  $2n^*$ . Arrows denote transitions between genotypes, with transition rates  $\mu$  for the beneficial mutation rate and  $\delta$  for the aneuploidy rate. Elevation differences illustrate the expected, rather than the assumed, fitness differences between the genotypes.

**Estimated rates and fitness effects of aneuploidy and mutation.** We inferred the posterior distribution of model parameters (Figure 2). We report parameter estimates using the MAP (maximum a posteriori) and providing the 50% HDI (highest density interval) in square brackets. See Supplementary Material for sensitivity analysis.  
 100  
 102

The estimated beneficial mutation rate is  $\mu = 2.965 \cdot 10^{-6}$  [ $2.718 \cdot 10^{-7} - 3.589 \cdot 10^{-6}$ ] per genome per generation. From the literature, the mutation rate per base pair is roughly  $2 - 3 \cdot 10^{-10}$  (refs. <sup>74,35</sup>), but it may be higher under heat stress, as several stresses<sup>20</sup>, including heat<sup>22</sup>, may cause hypermutation in yeast. If we assume a 10-fold increase over the mutation rate reported in the literature, then the estimated beneficial mutation rate can be explained by a genomic target size of 1,000 base pairs (that is, 1,000 base pairs across the genome in which a mutation would provide a fitness benefit). Supporting this, Jarolim et al.<sup>25</sup> found 279 genes that contributed to survival after a sudden shift from 30 °C to 50 °C, and Flynn et al.<sup>14</sup> used a deep mutational scan of a single protein, Hsp90, to find 465

amino-acid variants that increased growth rate in 37 °C. Furthermore, Yona et al.<sup>70</sup> found at least 10 genes on Chromosome III that increased heat tolerance when over-expressed. Assuming that other chromosomes also have a similar number of heat-tolerance genes (and even more, as Chromosome III is one of the smallest chromosomes<sup>18</sup>), we get a total of 160 heat-tolerance genes in the genome.

Indeed, mutations were found in 97 genes in an evolutionary experiment with yeast under heat stress<sup>22</sup>. Thus, to get a genomic target size of 1,000, it is enough that the average gene target size (number of base pairs in a gene in which a mutation is beneficial) is 6.25 base pairs. For example, Kohn and Anderson<sup>30</sup> found a target size of 11 in a proton exporter gene (*PMA1*) that contributes to high-salt adaptation.

The estimated aneuploidy rate,  $\delta = 1.72 \cdot 10^{-3}$  [ $1.47 \cdot 10^{-3} - 2.786 \cdot 10^{-3}$ ] is higher than in previous studies: for Chromosome III in diploid *S. cerevisiae*, Zhu et al.<sup>74</sup> estimated  $6.7 \cdot 10^{-6}$  chromosome gain events per generation, and Kumaran et al.<sup>32</sup> estimate  $3.0 \cdot 10^{-5} - 4.3 \cdot 10^{-5}$  chromosome loss events per generation (95% confidence interval). However, this difference may be partly explained by an increased aneuploidy rate during heat stress: heat shock can increase the rate of chromosome fragment loss by 2-3 orders of magnitude<sup>5</sup>.

The estimated fitness values are  $w_{2n+1} = 1.022$  [ $1.021 - 1.023$ ],  $w_{2n+1^*} = 1.025$  [ $1.024 - 1.026$ ],  $w_{2n^*} = 1.028$  [ $1.026 - 1.029$ ], all relative to the fitness of  $2n$ , which is set to  $w_{2n} = 1$ . Thus, we can infer that the cost of Chromosome III trisomy is  $c = w_{2n^*} - w_{2n+1^*} = 0.003$  (or 0.3%) and the benefit of trisomy is  $w_{2n+1} - 1 - c = 0.019$  (1.9%), whereas the benefit of the beneficial mutation is  $w_{2n^*} - 1 = 0.028$  (2.8%).

If we allow for transitions (mutation, chromosome loss and gain) to less-fit genotypes (e.g.,  $2n^*$  to  $2n+1^*$ ), then we infer similar but slightly different values, see Supplementary Material.

**Model comparison and goodness-of-fit.** To assess the fit of our model to the data, we use posterior predictive checks, in which we simulate the frequency dynamics using MAP parameter estimates and compare them to the data. Our model fits the data well:  $2n^*$  fixed in 63% of simulations by generation 1,700 and in 100% of simulations by generation 2,350 (Figure 3).

However, a model without aneuploidy (where the aneuploidy rate is fixed at zero,  $\delta = 0$ ), fails to explain the experimental observations (Figure 3). The estimated mutation rate without aneuploidy is  $\mu = 7.98 \cdot 10^{-9}$  [ $7.906 \cdot 10^{-9} - 8.138 \cdot 10^{-9}$ ], much lower compared to a model with aneuploidy. The fitness of the mutant is also much lower at  $w_{2n^*} = 1.013$  [ $1.012 - 1.013$ ]. This is because, without aneuploidy, a high mutation rate or fitness effect will lead to faster appearance and fixation of  $2n^*$  than

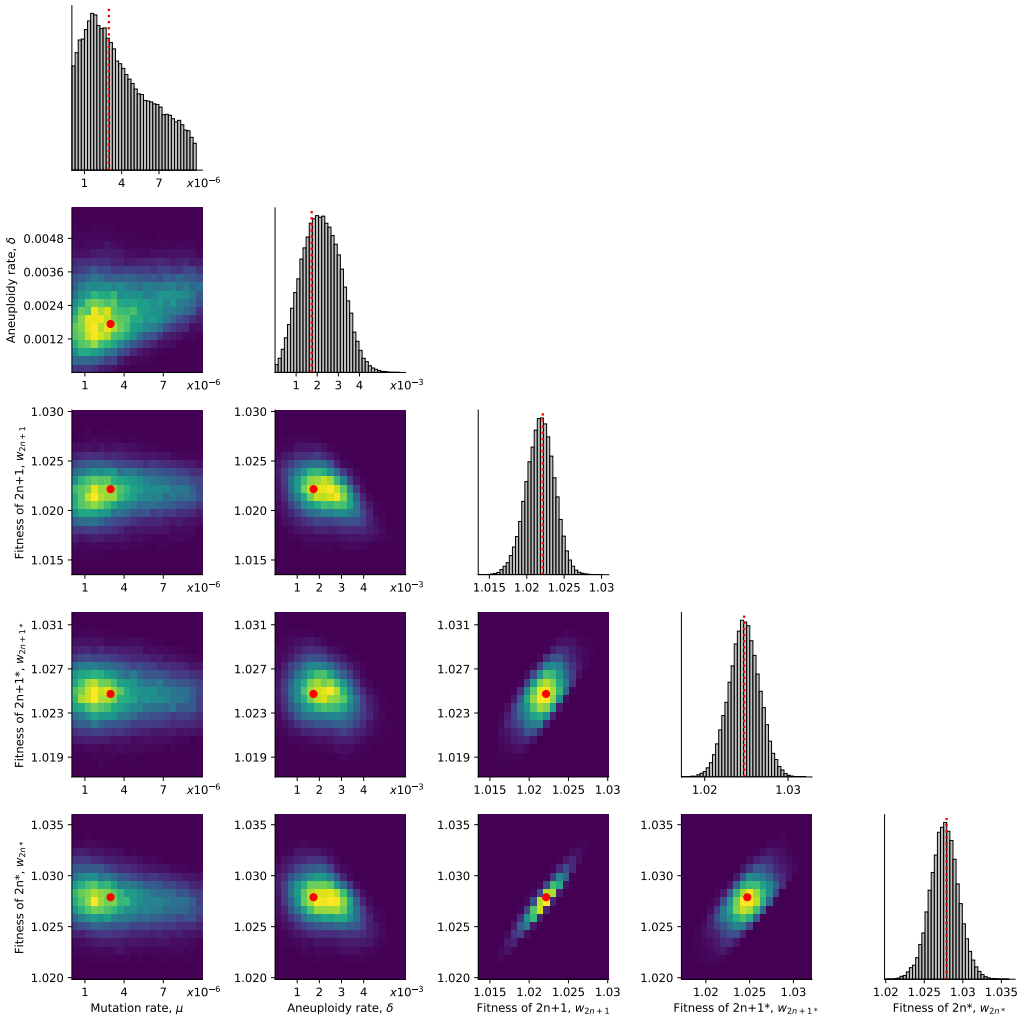


**Figure 2: Posterior distribution of model parameters.** On the diagonal, the marginal posterior distribution of each model parameter. Below the diagonal, the joint posterior distribution of pairs of model parameters (dark purple and bright yellow for low and high density, respectively). Red markers and orange lines for the joint MAP estimate (which may differ from the marginal MAP, as the marginal distribution integrates over all other parameters).

142 in the experimental observations.

We also checked a model in which aneuploidy occurs but is adaptively neutral compared to the wild-type, that is,  $w_{2n+1} = w_{2n}$  and  $w_{2n+1*} = w_{2n*}$  but  $\delta > 0$ . This model fits the data better than the model with no aneuploidy (in which  $\delta = 0$ ), but worse than a model with positive selection for aneuploidy, 146 in which  $w_{2n} < w_{2n+1} < w_{2n+1*} < w_{2n*}$  (Figure 3).

**Model predictions of genotype frequency dynamics.** We simulated 50 replicate genotype frequency dynamics using the MAP estimate parameters. Figure 4A shows the simulated frequencies of the four genotypes ( $2n$ ,  $2n+1$ ,  $2n+1^*$  and  $2n^*$ ), as well as the frequencies of  $2n^*$  cells that arose from 148 either  $2n+1$  cells via a sequences of mutation and chromosome loss events ( $2n_A^*$ ), or directly from 150 either  $2n+1$  cells via a sequences of mutation and chromosome loss events ( $2n_A^*$ ), or directly from

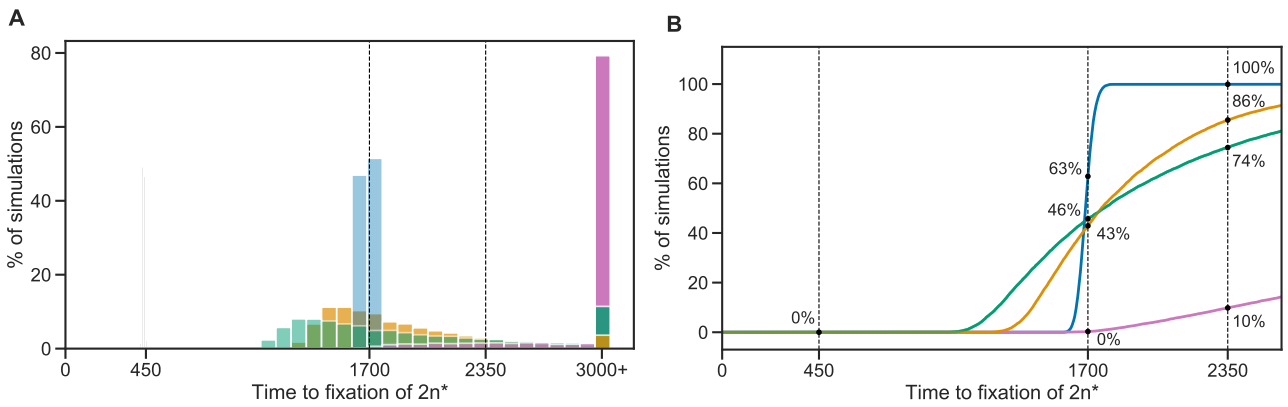


**Figure 3: Model fit with and without aneuploidy.** The distribution of time to fixation of  $2n^*$  (i.e., adaptation time) in 10,000 simulations using MAP parameters of the model with beneficial aneuploidy (blue;  $\delta > 0$ ,  $w_{2n} < w_{2n+1} < w_{2n+1}^* < w_{2n}^*$ ) compared to alternative models: a model with the same parameter values but without aneuploidy (gray,  $\delta = 0$ , concentrated at  $t = 450$ ); a model fitted to the data assuming no aneuploidy (green,  $\delta = 0$ ); a model fitted to the data assuming neutral aneuploidy (yellow,  $\delta > 0$ ,  $w_{2n+1} = w_{2n}$ ,  $w_{2n+1}^* = w_{2n}^*$ ); and a model with beneficial aneuploidy and an extended prior distribution (pink). In the experiment by Yona et al.<sup>70</sup>, one population lost aneuploidy by generation 1,700 and another by generation 2,350 (dashed lines) but not before generation 450. Thus, the blue distribution has a better fit compared to the other distributions (the gray distribution has a particularly poor fit). The MAP likelihood (eq. (4)) is 0.84, 0.78, 0.67, and 0.14 for the models represented by blue, yellow, green, and pink distributions, respectively. **(A)** Histogram of the time to fixation of  $2n^*$ . The last bin contains all values equal or greater than 3,000. **(B)** Cumulative distribution of the time to fixation.

2n cells via a mutation event ( $2n_M^*$ ). We find that  $2n+1^*$  never reaches substantial frequency as it is quickly replaced by  $2n^*$  in a process similar to *stochastic tunneling*<sup>24,31</sup>.

To test the hypothesis that aneuploidy facilitates adaptation, we estimated  $F_A$ , the expected frequency of  $2n^*$  that arose from  $2n+1$ , computed as the average frequency of such  $2n_A^*$  cells at the end of simulations using the MAP estimate parameters. Surprisingly, we observe that the majority of  $2n^*$  cells are  $2n_M^*$ , a product of a direct mutation in 2n cells, rather than descending from  $2n+1$  cells ( $F_A^{MAP} = 0.106$ , average end point of 50 purple lines in Figure 4A). This is despite the fact that the  $2n+1$  genotype reaches high frequencies in the population (at least 0.98, Figure 4A).

This result is not unique to the MAP parameter estimate. We simulated genotype frequency dynamics using parameter samples from the posterior distribution, and computed the posterior distribution of  $F_A$  (Figure 4B). The posterior mode  $F_A$  was just 0.147 [0.0154-0.370 95% CI] and only in 489 of 100,000 posterior samples (0.489%)  $F_A$  was larger than 0.5 (see Supporting Material for results when

transitions to less-fit genotypes are allowed, such as  $2n^*$  to  $2n+1^*$ ). Thus, if we sample a random  
164 cell from the evolved  $2n^*$  population, it is more likely to have descended directly from an euploid  
cell than from an aneuploid cell. The probability of  $2n^*$  descending from  $2n+1$  ( $F_A$ ) increases  
166 with the aneuploidy rate,  $\delta$ , and decreases with both the population size  $N$  and the mutation rate,  $\mu$   
(Figure 4C,D). In some cases it can also be affected by the fitness parameters (Figure S10).

168 **Genetic instability in aneuploid cells.** It has been suggested that aneuploidy increases genetic  
instability: Sheltzer et al.<sup>56</sup> have demonstrated a fold increase of between 2.2 and 7.1 in mutation  
170 rate. Therefore, we inferred model parameters under the assumption that the mutation rate increases  
in aneuploid cells by a factor  $\tau = 1, 33/32$  (due to an additional chromosome), 2, 5, 10, or 100 (due  
172 to genetic instability). We found that the posterior distribution was similar for  $\tau = 1, 33/32, 2$ , and 5  
(Figure S4). Furthermore, we computed the WAIC, a criterion for model selection (Methods). The  
174 WAIC values were similar for all  $\tau$  values (Table S1).

Assuming a strong increase of the mutation rate in aneuploid cells, i.e.  $\tau = 100$ , the inferred a  
176 mutation rate was  $\mu = 4.094 \cdot 10^{-7}$  [ $6.252 \cdot 10^{-8} - 6.046 \cdot 10^{-7}$ ]), and the inferred aneuploidy rate  
that was  $\delta = 0.744 \cdot 10^{-3}$  [ $0.506 \cdot 10^{-3} - 1.827 \cdot 10^{-3}$ ]. Compared to inference made assuming no  
178 effect of aneuploidy on the mutation rate, these rates were about 7-8-fold and 2-3-fold lower for  $\mu$  and  
 $\delta$ , respectively. Assuming  $\tau = 10$ , the inferred a mutation rate was only slightly lower compared to  
180  $\tau = 1$  ( $\mu = 1.67 \cdot 10^{-6}$  [ $2.836 \cdot 10^{-8} - 2.245 \cdot 10^{-6}$ ]).

Therefore, we do not find any evidence of an increase in mutation rate in aneuploid cells. This may  
182 be because, unless the increase is strong ( $\tau \geq 10$ ), it does not seem to affect our inference; or because  
Chromosome III is one of the smallest chromosomes<sup>18</sup>. We also checked the differences in genotype  
184 frequency dynamics for different  $\tau$  values. We observe  $\tau = 100$  could be distinguished if accurate  
data was available for the waiting time until the frequency of  $2n$  to decrease below 95% (Figure S5A)  
186 or for waiting time for the frequency of  $2n+1$  to either reach or go below 95% (Figure S5B). Similarly,  
we did not find evidence for an increase in the aneuploidy rate in aneuploid cells<sup>56</sup>, probably due to  
188 lack of statistical power.

## Discussion

190 In a study on the role of chromosome duplication in adaptive evolution, Yona et al.<sup>70</sup> found that a  
Chromosome III trisomy was acquired by *S. cerevisiae* populations evolving under heat stress, only  
192 to be later replaced by euploid mutant cells that carry "refined" solutions to the stress. Additionally,  
such a replacement also occurred when they initiated evolutionary experiments with a population in

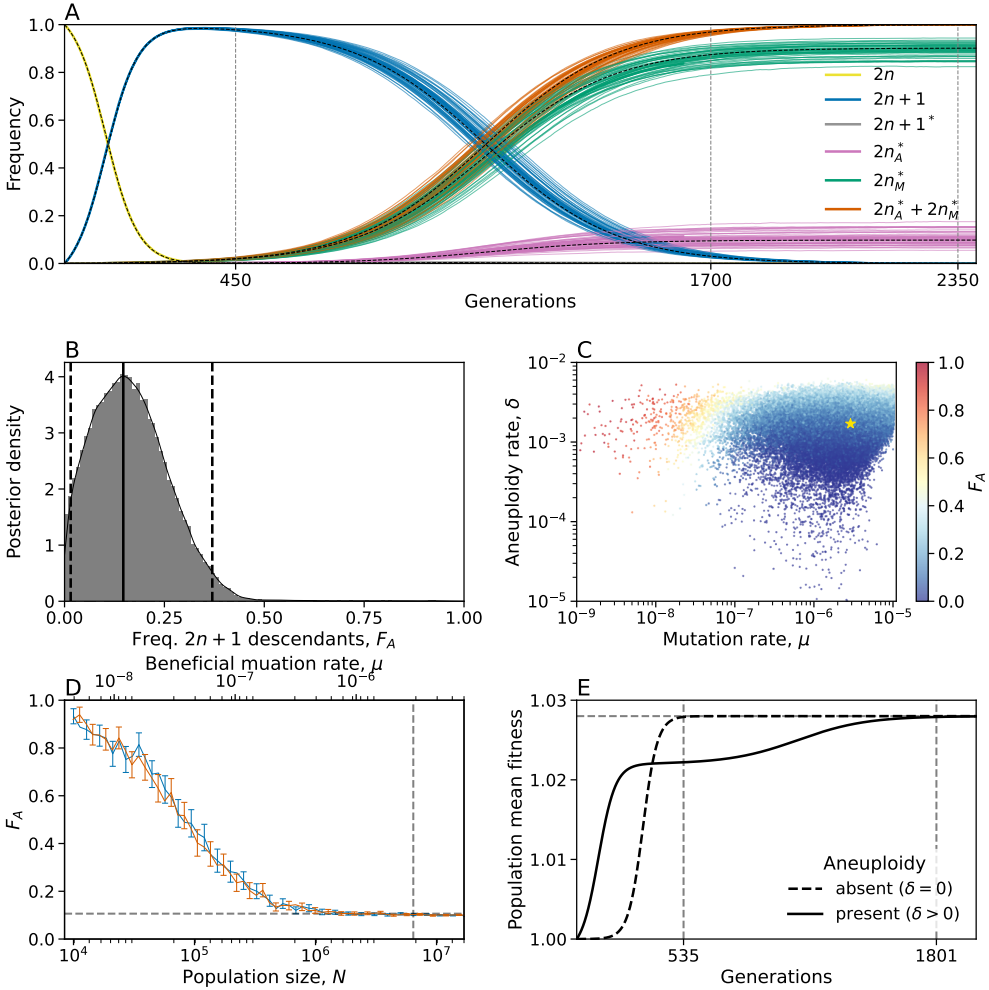


**Figure 4: Predicted frequency of aneuploid-descended cells.** **(A)** Posterior predicted genotype frequencies over time, including the source of  $2n^*$ :  $2n_A^*$  arose from  $2n + 1$ , whereas  $2n_M^*$  arose directly from  $2n$ . Colored curves are 50 simulations using the MAP estimate parameters. Black dashed curves are the expected genotype frequencies without genetic drift (from a deterministic model). See Figure S9 for log-log scale, in which the sequence of events is easier to observe. **(B)** Posterior distribution of  $F_A$ , the expected frequency of  $2n^*$  cells descended from  $2n+1$  cells, computed as the average frequency at the end of 100 simulations for 100,000 samples from the parameter posterior distribution. Solid and dashed lines show the mode and 95% CI. **(C)**  $F_A$  values (color coded) from panel B, with their corresponding mutation rate  $\mu$  on x-axis and aneuploidy rate  $\delta$  on the y-axis. Yellow star shows the MAP estimate. See also Figure S10. **(D)**  $F_A$  as a function of the population size ( $N$ , bottom x-axis) and the beneficial mutation rate ( $\mu$ , top x-axis) in posterior predictions with MAP parameters. Markers show  $F_A$  in 250 simulations per population size or mutation rate value. Error bars show mean  $F_A$  with 95% CI (bootstrap,  $n = 10,000$ ). Blue and red bars for varying population size and mutation rate, respectively. Vertical dashed line for population size in the experiment,  $6.425 \cdot 10^6$ , and the MAP mutation rate,  $2.965 \cdot 10^{-6}$ . Horizontal line for  $F_A^{MAP} = 0.106$ . **(E)** Population mean fitness in a model without drift using MAP estimate parameters. Solid lines for mean fitness with aneuploidy ( $\delta > 0$ ), where the population reaches adaptation (mean fitness at 99.99% of maximum value) at generation 1,802. Dashed lines for mean fitness without aneuploidy ( $\delta = 0$ ), where the population adapts much earlier, at generation 535.

194 which all cells carry a Chromosome III trisomy. They hypothesized that aneuploidy is a “useful yet  
195 short-lived intermediate that facilitates further adaptation”, suggesting that the euploid mutant cells  
196 evolved by heat-resistance mutations in aneuploid cells followed by reversion of trisomy due to a  
chromosome loss event.

198 We developed an evolutionary genetic model of adaptive evolution by aneuploidy and mutation  
(Figure 1), fitted it to the experimental results of Yona et al.<sup>70</sup>, and used it to predict the genotype  
200 frequency dynamics. The model predicted that only about 10-15% of the evolved euploid population  
descended from aneuploid cells by acquiring a mutation and losing the extra chromosome—that is,  
202 the majority of the euploid population are not descended from aneuploid cells, but rather are direct  
descendants of the ancestral wild-type population (Figure 4).

204 This happens despite aneuploidy reaching a high frequency in the population (>95%). Conventional  
wisdom might suggest that once the aneuploid genotype  $2n+1$  reaches high frequency, it will have a  
206 better chance at producing "refined" solutions via mutations, and its descendants will come to dominate  
the population: the frequency of  $2n_A^*$  (which arises from  $2n+1^*$ ) will be higher than the frequency of  
208  $2n_M^*$  (which arises directly from  $2n$ ).

So how does  $2n_M^*$  prevail? Initially, the supply rates of  $2n+1$  and  $2n_M^*$  are  $N\delta \approx 11,000$  and  $N\mu \approx 19$ ,  
210 respectively (assuming MAP parameter estimates). Therefore, both genotypes are expected to appear  
immediately at the beginning of the experiment (Figure S9). However,  $2n+1$  appears at a much higher  
212 frequency as  $\delta \gg \mu$  by 2-3 orders of magnitude. After they first appear,  $2n_M^*$  has higher fitness. But  
as long as the frequency of  $2n$  is high, the supply rate of  $2n+1$  is higher than that of  $2n_M^*$ , again due to  
214  $\delta \gg \mu$ . However, supply rates of both genotypes decrease with the frequency of  $2n$ . Therefore, when  
the latter decreases, mainly due to the increase in the frequency of  $2n+1$ , both supply rates diminish.  
216 At this stage, the higher fitness of  $2n_M^*$  comes into play and it starts to take over the population, which  
is mainly composed of  $2n+1$ . For the aneuploid lineage to compete with the mutant lineage, it must  
218 produce  $2n_A^*$  via a mutation followed by chromosome loss. Although this is a stochastic process  
(due to drift), our results show that the time until  $2n_A^*$  reaches a frequency of 0.1% is roughly 450  
220 generations, without much variation (intersection of purple lines and vertical dashed line in Figure S9).  
However, by that time  $2n_M^*$  is already at a roughly 10-fold higher frequency (1.86%), and since both  
222 mutants have the same fitness, their relative frequency remains roughly the same until the end of the  
experiment.

224 **Predictions for small populations and low mutation rates.** We examined the effect of the popula-  
tion size,  $N$ , and the beneficial mutation rate,  $\mu$ , on the frequency of  $2n+1$  descendants in the evolved

226 population,  $F_A$ . We found that  $F_A$  is expected to decrease as the population size or mutation rate  
increase (Figure 4D), ranging from >90% when the population size is 10,000 or the mutation rate is  
228  $6 \cdot 10^{-9}$ , to about 10% when the population size is above 1,000,000 (less than the experimental popu-  
lation size, which was 6,425,000) or the mutation rate is above  $2 \cdot 10^{-6}$  (less than the inferred mutation  
230 rate, which is  $2.965 \cdot 10^{-6}$ ). Thus, our model provides a testable prediction: if the experiment was  
repeated under a lower population size (via stronger daily dilutions or in a smaller volume) or a lower  
232 mutation rate (via a non-mutagenic stress or stress with a smaller target size such as drug resistance),  
then the fraction of the population descending from aneuploid cells would be much higher.

234 **Aneuploidy delays rather than facilitates adaptation.** An additional interesting result of our  
study is that aneuploidy increases, rather than decreases, the adaptation time (Figure 4E). This  
236 happens despite the fact that the mean fitness initially increases faster in the presence of aneuploidy  
(Figure 4E). This is because once  $2n+1$  is common, selection for the mutant strain ( $2n+1^*$  or  $2n^*$ ) is  
238 weaker compared to when  $2n^*$  competes directly with  $2n$ .

**Rate and fitness effect of aneuploidy and mutation.** We inferred the rates of aneuploidy and  
240 mutation and their effects on fitness. We estimate that the aneuploidy rate (i.e., number of chromosome  
gains per generation) is  $1.7 \cdot 10^{-3}$ , higher than a previous estimate of  $6.7 \cdot 10^{-6}$  (ref 73). This may be due  
242 to genetic instability caused by heat stress<sup>5</sup>. In addition, we find no evidence for increased mutation  
rates in aneuploid cells. Previous empirical studies have suggested that genetic instability (e.g.,  
244 elevated mutation rates) in aneuploid cells is due to stress associated with the aneuploid state<sup>3,6,71,23</sup>.  
However, in the experiment of Yona et al.<sup>70</sup>, both the wild-type and the aneuploid were under heat  
246 stress, which may explain why we did not find evidence for an increased mutation rate specifically in  
aneuploid cells.

248 **Conclusions.** Here, we tested the hypothesis that aneuploidy cells are an evolutionary "stepping  
stone", or adaptive intermediate, between wild-type euploid cells and mutant euploid cells<sup>69</sup>. Our  
250 results suggest that, although it seems the population goes from euploid to aneuploid and back, this is  
not the case at the individual level. We estimate that only about 10-15% of the euploid cells descended  
252 from aneuploid cells, whereas the rest are direct descendants of the wild-type euploid cells. Thus,  
aneuploidy can delay, rather than accelerate, adaptation, and cells that become aneuploid may leave  
254 less descendants than cells that remain euploid. This surprising result reinforces the importance of  
mathematical models when interpreting evolutionary dynamics. Moreover, our study emphasizes the  
256 unintuitive outcomes of clonal interference between mechanisms for generation of variation that differ

in their rate of formation and distribution of fitness effects, including mutation, copy number variation,

258 horizontal gene transfer, and epigenetic modifications.

## Models and Methods

260 **Evolutionary genetic model.** We model the evolution of a population of cells using a Wright-Fisher model<sup>40</sup>, assuming a constant effective population size  $N$ , non-overlapping generations, and  
262 including the effects of natural selection, genetic drift, aneuploidy, and mutation. We focus on beneficial genetic modifications, neglecting the effects of deleterious and neutral mutations or karyotypic  
264 changes. The model allows for a single aneuploid karyotype (e.g., Chromosome III duplication) and a single mutation to accumulate in the genotype. Thus, the model follows four genotypes (Figure 1):  
266 euploid wild-type,  $2n$ , the initial genotype; euploid mutant,  $2n^*$ , with the standard karyotype and a single beneficial mutation; aneuploid wild-type,  $2n+1$ , with an extra chromosome, i.e., following  
268 chromosome duplication; and aneuploid mutant,  $2n+1^*$ , with an extra chromosome and a beneficial mutation.

270 Transitions between the genotypes occur as follows (Figure 1): Beneficial mutations from  $2n$  to  $2n^*$  and from  $2n+1$  to  $2n+1^*$  occur with probability  $\mu$ , the mutation rate. We neglect back-mutations (i.e.,  
272 from  $2n^*$  to  $2n$  and from  $2n+1^*$  to  $2n+1$ ). Aneuploidy is formed by chromosome mis-segregation,  
274 so that cells transition from  $2n$  to  $2n+1$  and from  $2n+1^*$  to  $2n^*$  with probability  $\delta$ , the aneuploidy rate. That is, we assume chromosomes are gained and lost at the same rate, and we neglect events  
276 that form a less-fit genotype (i.e.,  $2n+1$  to  $2n$  and  $2n^*$  to  $2n+1^*$ ). A model that assumed increased  
of statistical power, and was abandoned.

278 In the experiment by Yona et al.<sup>70</sup>, the population was grown every day from  $1.6 \cdot 10^6$  cells until reaching stationary phase and then diluted 1:120. Thus, we set the population size to  $N = 6.425 \cdot 10^6$ ,  
280 the harmonic mean of  $\{2^k \cdot 1.6 \cdot 10^6\}_{k=0}^7$ <sup>10</sup>. The initial population has  $N$  cells with genotype  $2n$ .  
The effect of natural selection on the frequency  $f_i$  of genotype  $i = 2n, 2n+1, 2n+1^*$ , or  $2n^*$  is given  
282 by

$$f_i^s = \frac{f_i w_i}{\bar{w}} , \quad (1)$$

284 where  $w_i$  is the fitness of genotype  $i$  and  $\bar{w} = \sum_j f_j w_j$  is the population mean fitness. The effect of

mutation and aneuploidy on genotype frequencies is given by

$$\begin{aligned}
 f_{2n}^m &= (1 - \delta - \mu) f_{2n}^s, \\
 f_{2n+1}^m &= \delta f_{2n}^s + (1 - \mu) f_{2n+1}^s, \\
 f_{2n+1^*}^m &= \mu f_{2n+1}^s + (1 - \delta) f_{2n+1^*}^s, \\
 f_{2n^*}^m &= \mu f_{2n}^s + \delta f_{2n+1}^s + f_{2n^*}^s.
 \end{aligned} \tag{2}$$

Finally, random genetic drift is modeled using a multinomial distribution<sup>40</sup>,

$$\mathbf{f}' \sim \frac{1}{N} \cdot \text{Mult}(N, \mathbf{f}^m), \tag{3}$$

where  $\mathbf{f}^m = (f_{2n}^m, f_{2n+1}^m, f_{2n+1^*}^m, f_{2n^*}^m)$  are the frequencies of the genotypes after mutation and aneuploidy,  $\mathbf{f}'$  are the genotype frequencies in the next generation, and  $\text{Mult}(N, \mathbf{f})$  is a multinomial distribution parameterized by the population size  $N$  and the genotype frequencies  $\mathbf{f}$ . Overall, the change in genotype frequencies from one generation to the next is given by the transformation  $f_i \rightarrow f'_i$ .

**Empirical data for model inference.** We use the results of evolutionary experiments reported by

Yona et al.<sup>70</sup>. In their heat-stress experiment, four populations of *S. cerevisiae* evolved under 39 °C. Aneuploidy fixed in all four population in the first 450 generations. Hereafter, fixation or elimination of a genotype *by generation t* means that more than 95% or less than 5% of the population carry the genotype at generation  $t$ , and possibly earlier. From re-analysis of data not published in the original paper, aneuploidy did not fix before at least 200 generations elapsed. The experiment continued with two populations, in which aneuploidy was eliminated by generation 1,700 and 2,350 while still under the same conditions of elevated heat (39 °C).

**Likelihood function.** Because our model, just like the Wright-Fisher model, is non-linear and

stochastic, computing the distribution of fixation time  $T(g)$  of genotype  $g$  for use in the likelihood function is intractable (it is even hard to use a diffusion-equation approximation due to the model having multiple genotypes, rather than just two). We overcome this problem by approximating the likelihood using simulations. We simulate 1,000 experiments per parameter vector  $\theta = (\mu, \delta, s, b, c)$ , resulting in a set of simulated observations  $\tilde{\mathbf{X}} = \{\tilde{X}_i\}_{i=1}^{1000}$ . We then compute the approximate likelihood,

$$\begin{aligned}
 \mathcal{L}(\theta) = P^4(200 \leq T(2n+1) \leq 450) \cdot & \left[ 1 - \right. \\
 & P_{\tilde{\mathbf{X}}}^4(\{T(2n^*) < 1700\} \mid 200 \leq T(2n+1) \leq 450) - \\
 & P_{\tilde{\mathbf{X}}}^4(\{1700 < T(2n^*) < 2350\} \mid 200 \leq T(2n+1) \leq 450) + \\
 & \left. P_{\tilde{\mathbf{X}}}^4(\{T(2n^*) < 1700\} \wedge \{1700 < T(2n^*) < 2350\} \mid 200 \leq T(2n+1) \leq 450) \right], \tag{4}
 \end{aligned}$$

308 where  $!\{\dots\}$  is the "logical not" operator,  $P^4(\dots)$  is the 4th power of  $P(\dots)$ , and all probabilities  
 $P_{\tilde{\mathbf{X}}}(\dots)$  are approximated from the results of the simulations  $\tilde{\mathbf{X}}$ . For example,  $P_{\tilde{\mathbf{X}}}(!\{T(2n^*) < 1700\} |$   
310  $200 \leq T(2n+1) \leq 450)$  is approximated by taking simulations in which  $2n+1$  fixed before generation  
450 but not before generation 200, and computing the fraction of such simulations in which  $2n^*$  did  
312 not fix by generation 1,700, and hence aneuploidy did not extinct before generation 1,700. Figure S1  
compares results with less and more simulated experiments, demonstrating that 1,000 simulations are  
314 likely sufficient.

For a model without aneuploidy (that is, when the aneuploidy rate is fixed at zero,  $\delta = 0$ ), we disregard  
316 the increased expression in Chromosome III and the growth advantage measured in generation 450,  
and focus on the growth advantage measured in later generations, presumably due to a beneficial  
318 mutation. Therefore, the likelihood is approximated by

$$\begin{aligned}\mathcal{L}_!(\theta) = 1 - P_{\tilde{\mathbf{X}}}^4(!\{T(2n^*) < 1700\}) - \\ P_{\tilde{\mathbf{X}}}^4(!\{1700 < T(2n^*) < 2350\}) + \\ P_{\tilde{\mathbf{X}}}^4(!\{T(2n^*) < 1700\} \wedge !\{1700 < T(2n^*) < 2350\}).\end{aligned}\quad (5)$$

320 **Parameter inference.** To infer model parameters, we use approximate Bayesian computation with  
a sequential Monte-Carlo scheme, or ABC-SMC<sup>59</sup>, implemented in the pyABC Python package<sup>29</sup>  
322 [pyabc.readthedocs.io](https://pyabc.readthedocs.io). This approach uses numerical stochastic simulations of the model to infer  
a posterior distribution over the model parameters. It is a method of likelihood-free, simulation-  
324 based inference<sup>9</sup>, that is, for estimating a posterior distribution when a likelihood function cannot be  
directly computed. It is therefore suitable in our case, in which the likelihood function can only be  
326 approximated from simulations, and cannot be directly computed.

The ABC-SMC algorithm employs sequential importance sampling over multiple iterations<sup>63,28,61</sup>. In  
328 iteration  $t$  of the algorithm, a set of parameter vectors,  $\{\theta_{i,t}\}_{i=1}^{n_t}$ , also called *particles*, are constructed  
in the following way. A proposal particle,  $\theta^*$ , is sampled from a proposal distribution, and is either  
330 accepted or rejected, until  $n_t$  particles are accepted. The number of particles,  $n_t$ , is adapted at every  
iteration  $t$  using the adaptive population strategy<sup>29</sup> [pyabc.readthedocs.io](https://pyabc.readthedocs.io). For  $t = 0$ , the proposal  
332 particle is sampled from the prior distribution,  $p(\theta)$ . For  $t > 0$ , the proposal particle is sampled from  
the particles accepted in the previous iteration,  $\{\theta_{i,t-1}\}_{i=1}^{n_{t-1}}$ , each with a probability relative to its weight  
334  $W_{t-1}(\theta_{i,t-1})$  (see below). The proposal particle is then perturbed using a kernel perturbation kernel,  
 $K_t(\theta^* | \theta)$  where  $\theta$  is the sample from the previous iteration. Then, a set of synthetic observations  
336  $\tilde{\mathbf{X}}^*$  is simulated, and the proposal particle  $\theta^*$  is accepted if its approximate likelihood (eq. (4)) is high  
enough,  $\mathcal{L}(\theta^*) > 1 - \epsilon_t$  (or more commonly, if  $1 - \mathcal{L}(\theta^*) < \epsilon_t$ ), where  $\epsilon_t > 0$  is the *acceptance*

338 *threshold*, as higher values of  $\epsilon_t$  allow more particles to be accepted. The acceptance threshold  $\epsilon_t$  is  
339 chosen as the median of the  $1 - \mathcal{L}(\theta)$  of the particles accepted in the previous iteration,  $t - 1$ , and  
340  $\epsilon_0 = 0.01$ . For each accepted particle  $\theta_{i,t}$  a weight  $W_t(\theta_{i,t})$  is assigned: for  $t = 0$ ,  $W_0(\theta_{i,0}) = 1$ ,  
341 and for  $t > 0$ ,  $W_t(\theta_{i,t}) = p(\theta_{i,t}) / \sum_{i=1}^{n_{t-1}} W_{t-1}(\theta_{i,t-1}) K_t(\theta_{i,t}, \theta_{i,t-1})$ , where  $p(\theta)$  is the prior density of  
342  $\theta$  and  $K_t(\theta', \theta)$  is the probability of a perturbation from  $\theta$  to  $\theta'$ .  $K_t(\theta' | \theta)$  is a multivariate normal  
343 distribution, fitted at iteration  $t$  to the particles from the previous iteration,  $\{\theta_{i,t-1}\}_{i=1}^{n_{t-1}}$ , and their  
344 weights,  $\{W(\theta_{i,t-1})\}_{i=1}^{n_{t-1}}$ .

Acceptance is determined according to the approximate likelihood (eq. (4)), which has a maximum  
345 value of  $\mathcal{L}_{max} = 0.875$  (giving a minimal value of  $\epsilon_{min} = 0.125$ ). We terminated the inference  
346 iterations when the change in  $\epsilon$  value from one iteration to the next was small. With our standard prior  
347 and model, we reached  $\epsilon = 0.13$  (or  $\mathcal{L} = 0.87$ ) after six iterations, with  $n_6 = 982$  accepted parameter  
348 vectors and effective sample size ESS=651 (Figure S2). Running the inference algorithm with different  
349 initialization seeds and less or more simulations for approximating the likelihood produced similar  
350 posterior distributions (Figure S1).

352 After producing a set of weighted particles from the the posterior distribution using the above ABC-  
353 SMC algorithm, we approximate the posterior using kernel density estimation (KDE) with Gaussian  
354 kernels. We truncate the estimated posterior to avoid positive posterior density for values with zero  
355 prior density. The MAP (maximum a posteriori) estimate is computed as the the maximum of the  
356 estimated joint posterior density. We then draw 5,000,000 samples from the posterior distribution  
357 to compute the HDI (highest density interval) and draw 50,000 samples to visualize the posterior  
358 distribution with histograms.

**Model comparison.** We examine several versions of our evolutionary models, e.g. without aneuploidy or with increased mutation rate in aneuploid cells, as well as several different prior distributions  
360 (see below). To compare these, we plot posterior predictions: for each model we execute 10,000  
361 simulations using the MAP parameter estimates and plot the distributions of time to fixation of  $2n^*$ ,  
362 one of key properties of the model likelihood. These plots visualize the fit of each model to the  
363 data. Also, for similar models we plot the marginal and joint posterior distributions of the parameters;  
364 if these are similar, we consider the models interchangeable. We validate this by comparing HDI  
365 (highest density interval) of posterior distributions.

Where posterior plots are very similar and the number of parameters is the same, we use WAIC, or

368 the widely applicable information criterion<sup>15</sup>, defined as

$$WAIC(\theta) = -2 \log \mathbb{E}[\mathcal{L}(\theta)] + 2\mathbb{V}[\log \mathcal{L}(\theta)] \quad (6)$$

370 where  $\theta$  is a parameter vector, and  $\mathbb{E}[\cdot]$  and  $\mathbb{V}[\cdot]$  are the expectation and variance taken over the  
372 posterior distribution, which in practice are approximated using 50,000 samples from the posterior  
374 KDE. We validated that upon resampling WAIC values do not significantly change and that differences  
imply higher predictive accuracy.

**Prior distributions.** We used informative prior distributions for  $w_{2n+1} = 1 - c + b$ ,  $w_{2n+1*} = (1 +$   
376  $s)(1 - c) + b$  and  $w_{2n*} = 1 + s$ , which we estimated from growth curves data from mono-culture growth  
experiments previously reported by Yona et al.<sup>70</sup>, Figs. 3C, 4A, and S2. We used Curveball, a method  
378 for predicting results of competition experiments from growth curve data<sup>43</sup> [curveball.yoavram.com](http://curveball.yoavram.com).  
Briefly, Curveball takes growth curves of two strains growing separately in mono-culture and predicts  
380 how they would grow in a mixed culture, that is, it predicts the results of a competition assay. From these  
predictions, relative fitness values can be computed. Because Curveball uses a maximum-likelihood  
382 approach to estimate model parameters, we were able to estimate a distribution of relative fitness  
values to be used as a prior distribution by sampling 10,000 samples from a truncated multivariate  
384 normal distribution defined by the maximum-likelihood covariance matrix (Figure S3).

We used growth curves of  $2n$  and  $2n+1$  in 39 °C to estimate an informative prior distribution for  
386  $w_{2n+1}$  (Figure S3-D, assuming  $w_{2n} = 1$ ). In this prior distribution, we used the same prior for  $w_{2n+1*}$   
and  $w_{2n*}$ . To increase computational efficiency, we also assumed  $w_{2n*} > w_{2n+1*} > w_{2n+1} > w_{2n}$ ;  
388 running the inference without this assumption produced similar results. See *supporting material* for  
an extended informative prior distribution that uses growth curves of  $2n*$  and  $2n+1$  growing in 39 °C;  
390 this prior distribution proved to be less useful.

As a control, we tested an uninformative uniform prior with  $U(1, 6)$ , for (i) all  $w_{2n+1}$ ,  $w_{2n+1*}$ ,  $w_{2n*}$ ,  
392 or (ii) only for  $w_{2n+1*}$ ,  $w_{2n*}$ , using the above informative prior for  $w_{2n+1}$ . In these cases the inference  
algorithm failed to converge.  
394 For the mutation rate,  $\mu$ , and aneuploidy rate,  $\delta$ , we used uninformative uniform priors,  $\mu \sim$   
 $U(10^{-9}, 10^{-5})$  and  $\delta \sim U(10^{-6}, 10^{-2})$ . A wider mutation rate prior,  $\mu \sim U(10^{-9}, 10^{-3})$ , produced  
396 similar results.

## Acknowledgements

398 We thank Lilach Hadany, Judith Berman, David Gresham, Shay Covo, Martin Kupiec, Uri Obolski, Daniel  
Weissman, and Tal Simon for discussions and comments. This work was supported in part by the Israel  
400 Science Foundation (ISF, YR 552/19), the US–Israel Binational Science Foundation (BSF, YR 2021276),  
Minerva Center for Live Emulation of Evolution in the Lab (YR, YP), Minerva Stiftung short-term research  
402 grant (MP).

## References

- 404 [1] Avecilla, G., Chuong, J. N., Li, F., Sherlock, G., Gresham, D. and Ram, Y. 2022, ‘Neural  
networks enable efficient and accurate simulation-based inference of evolutionary parameters  
406 from adaptation dynamics’, *PLOS Biology* **20**(5), e3001633.
- 408 [2] Bakhoum, S. F. and Landau, D. A. 2017, ‘Chromosomal instability as a driver of tumor hetero-  
geneity and evolution’, *Cold Spring Harb. Perspect. Med.* **7**(6), 1–14.
- 410 [3] Bouchonville, K., Forche, A., Tang, K. E. S., Semple, C. a. M. and Berman, J. 2009, ‘Aneuploid  
chromosomes are highly unstable during dna transformation of *Candida albicans*.’, *Eukaryot.  
Cell* **8**(10), 1554–66.
- 412 [4] Boveri, T. 2008, ‘Concerning the origin of malignant tumours’, *J. Cell Sci.* **121**(Supplement  
1), 1–84.
- 414 [5] Chen, G., Bradford, W. D., Seidel, C. W. and Li, R. 2012, ‘Hsp90 stress potentiates rapid cellular  
adaptation through induction of aneuploidy.’, *Nature* **482**(7384), 246–50.
- 416 [6] Chen, G., Rubinstein, B. and Li, R. 2012, ‘Whole chromosome aneuploidy: Big mutations drive  
adaptation by phenotypic leap’, *BioEssays* **34**(10), 893–900.
- 418 [7] Cherry, J. M., Hong, E. L., Amundsen, C., Balakrishnan, R., Binkley, G., Chan, E. T., Christie,  
K. R., Costanzo, M. C., Dwight, S. S., Engel, S. R. et al. 2012, ‘Saccharomyces genome database:  
420 the genomics resource of budding yeast’, *Nucleic acids research* **40**(D1), D700–D705.
- 422 [8] Covo, S., Puccia, C. M., Argueso, J. L., Gordenin, D. A. and Resnick, M. A. 2014, ‘The sister  
chromatid cohesion pathway suppresses multiple chromosome gain and chromosome amplification.’,  
*Genetics* **196**(2), 373–384.
- 424 [9] Cranmer, K., Brehmer, J. and Louppe, G. 2020, ‘The frontier of simulation-based inference’,  
*Proceedings of the National Academy of Sciences* p. 201912789.

- 426 [10] Crow, J. F. and Kimura, M. 1970, *An introduction to population genetics theory*, Burgess Pub.  
Co., Minneapolis.
- 428 [11] Dhar, R., Sägesser, R., Weikert, C., Yuan, J. and Wagner, A. 2011, ‘Adaptation of *Saccharomyces cerevisiae* to saline stress through laboratory evolution.’, *J. Evol. Biol.* **24**(5), 1135–53.
- 430 [12] Dunham, M. J., Badrane, H., Ferea, T., Adams, J., Brown, P. O., Rosenzweig, F. and Botstein,  
D. 2002, ‘Characteristic genome rearrangements in experimental evolution of *Saccharomyces cerevisiae*’, *Proc. Natl. Acad. Sci.* **99**(25), 16144–16149.
- 432 [13] Elde, Nels, C., Child, Stephanie, J., Eickbush, Michael, T., Kitzman, Jacob, O., Rogers, Kelsey,  
S., Shendure, J., Geballe, Adam, P. and Malik, Harmit, S. 2012, ‘Poxviruses deploy genomic accordions to adapt rapidly against host antiviral defenses’, *Cell* **150**(4), 831–841.
- 436 [14] Flynn, J. M., Rossouw, A., Cote-Hammarlof, P., Fragata, I., Mavor, D., Hollins, C., Bank, C.  
and Bolon, D. N. 2020, ‘Comprehensive fitness maps of hsp90 show widespread environmental  
438 dependence’, *Elife* **9**, 1–25.
- [15] Gelman, A., Carlin, J. B., Stern, H. S., Dunson, D. B., Vehtari, A. and Rubin, D. B. 2013,  
440 *Bayesian Data Analysis, Third Edition*, Chapman & Hall/CRC Texts in Statistical Science,  
Taylor & Francis.
- 442 [16] Gerstein, A. C. and Berman, J. 2020, ‘*Candida albicans* genetic background influences mean and  
heterogeneity of drug responses and genome stability during evolution in fluconazole’, *mSphere*  
444 **5**(3).
- 446 [17] Gerstein, A. C., Ono, J., Lo, D. S., Campbell, M. L., Kuzmin, A. and Otto, S. P. 2015, ‘Too  
much of a good thing: the unique and repeated paths toward copper adaptation.’, *Genetics*  
**199**(2), 555–71.
- 448 [18] Gilchrist, C. and Stelkens, R. 2019, ‘Aneuploidy in yeast: Segregation error or adaptation  
mechanism?’, *Yeast* **36**(9), 525–539.
- 450 [19] Gresham, D., Desai, M. M., Tucker, C. M., Jenq, H. T., Pai, D. A., Ward, A., DeSevo, C. G.,  
Botstein, D. and Dunham, M. J. 2008, ‘The repertoire and dynamics of evolutionary adaptations  
452 to controlled nutrient-limited environments in yeast’, *PLoS Genet.* **4**(12).
- [20] Heidenreich, E. 2007, ‘Adaptive Mutation in *Saccharomyces cerevisiae*’, *Crit. Rev. Biochem.  
Mol. Biol.* **42**(4), 285–311.

- 456 [21] Hong, J. and Gresham, D. 2014, ‘Molecular specificity, convergence and constraint shape adaptive evolution in nutrient-poor environments’, *PLoS Genet.* **10**(1).
- 458 [22] Huang, C. J., Lu, M. Y., Chang, Y. W. and Li, W. H. 2018, ‘Experimental Evolution of Yeast for High-Temperature Tolerance’, *Mol. Biol. Evol.* **35**(8), 1823–1839.
- 460 [23] Ippolito, M. R., Martis, V., Martin, S., Tijhuis, A. E., Hong, C., Wardenaar, R., Dumont, M., Zerbib, J., Spierings, D. C., Fachinetti, D., Ben-David, U., Fojer, F. and Santaguida, S. 2021, ‘Gene copy-number changes and chromosomal instability induced by aneuploidy confer resistance to chemotherapy’, *Dev. Cell* **56**(17), 2440–2454.e6.
- 462 [24] Iwasa, Y., Michor, F. and Nowak, M. A. 2004, ‘Stochastic tunnels in evolutionary dynamics’, *Genetics* **166**(3), 1571–1579.
- 464 [25] Jarolim, S., Ayer, A., Pillay, B., Gee, A. C., Phrakaysone, A., Perrone, G. G., Breitenbach, M. and Dawes, I. W. 2013, ‘Saccharomyces cerevisiae genes involved in survival of heat shock’, *G3 Genes, Genomes, Genetics* **3**(12), 2321–2333.
- 468 [26] Kass, R. E. and Raftery, A. E. 1995, ‘Bayes factors’, *J. Am. Stat. Assoc.* **90**(430), 773.
- 470 [27] Kasuga, T., Bui, M., Bernhardt, E., Swiecki, T., Aram, K., Cano, L. M., Webber, J., Brasier, C., Press, C., Grünwald, N. J., Rizzo, D. M. and Garbelotto, M. 2016, ‘Host-induced aneuploidy and phenotypic diversification in the sudden oak death pathogen *Phytophthora ramorum*’, *BMC Genomics* **17**(1), 1–17.
- 472 [28] Klinger, E. and Hasenauer, J. 2017, A scheme for adaptive selection of population sizes in approximate bayesian computation - sequential monte carlo, in J. Feret and H. Koepll, eds, ‘Computational Methods in Systems Biology’, Vol. 10545, Springer International Publishing, pp. 128–144. Series Title: Lecture Notes in Computer Science.
- 474 [29] Klinger, E., Rickert, D. and Hasenauer, J. 2018, ‘pyabc: distributed, likelihood-free inference’, *Bioinformatics* (May), 1–3.
- 476 [30] Kohn, L. M. and Anderson, J. B. 2014, ‘The underlying structure of adaptation under strong selection in 12 experimental yeast populations’, *Eukaryot. Cell* **13**(9), 1200–1206.
- 478 [31] Komarova, N. L., Sengupta, A. and Nowak, M. A. 2003, ‘Mutation-selection networks of cancer initiation: Tumor suppressor genes and chromosomal instability’, *Journal of Theoretical Biology* **223**(4), 433–450.

- 484 [32] Kumaran, R., Yang, S.-Y. and Leu, J.-Y. 2013, ‘Characterization of chromosome stability in  
diploid, polyploid and hybrid yeast cells’, *PLoS ONE* **8**(7), e68094.
- 486 [33] Lauer, S., Avecilla, G., Spealman, P., Sethia, G., Brandt, N., Levy, S. F. and Gresham, D. 2018,  
‘Single-cell copy number variant detection reveals the dynamics and diversity of adaptation.’,  
488 *PLOS Biology* **16**.
- 490 [34] Lukow, D. A., Sausville, E. L., Suri, P., Chunduri, N. K., Wieland, A., Leu, J., Smith, J. C., Girish,  
492 V., Kumar, A. A., Kendall, J., Wang, Z., Storchova, Z. and Sheltzer, J. M. 2021, ‘Chromosomal  
instability accelerates the evolution of resistance to anti-cancer therapies’, *Developmental Cell*  
492 **56**(17), 2427–2439.e4.
- 494 [35] Lynch, M., Sung, W., Morris, K., Coffey, N., Landry, C. R., Dopman, E. B., Dickinson, W. J.,  
496 Okamoto, K., Kulkarni, S., Hartl, D. L. and Thomas, W. K. 2008, ‘A genome-wide view of the  
spectrum of spontaneous mutations in yeast’, *Proceedings of the National Academy of Sciences*  
496 **105**(27), 9272–9277.
- 500 [36] Mannaert, A., Downing, T., Imamura, H. and Dujardin, J. C. 2012, ‘Adaptive mechanisms in  
pathogens: Universal aneuploidy in *Leishmania*’, *Trends Parasitol.* **28**(9), 370–376.
- 502 [37] Möller, M., Habig, M., Freitag, M. and Stukenbrock, E. H. 2018, ‘Extraordinary genome  
504 instability and widespread chromosome rearrangements during vegetative growth’, *Genetics*  
500 **210**(2), 517–529.
- 508 [38] Naylor, R. M. and van Deursen, J. M. 2016, ‘Aneuploidy in cancer and aging’, *Annu. Rev. Genet.*  
508 **50**(1), 45–66.
- 512 [39] Niwa, O., Tange, Y. and Kurabayashi, A. 2006, ‘Growth arrest and chromosome instability in  
aneuploid yeast’, *Yeast* **23**(13), 937–950.
- 516 [40] Otto, S. P. and Day, T. 2007, *A biologist’s guide to mathematical modeling in ecology and  
evolution*, Princeton University Press.
- 520 [41] Pavelka, N., Rancati, G., Zhu, J., Bradford, W. D., Saraf, A., Florens, L., Sanderson, B. W., Hat-  
tem, G. L. and Li, R. 2010, ‘Aneuploidy confers quantitative proteome changes and phenotypic  
520 variation in budding yeast.’, *Nature* **468**(7321), 321–5.
- 524 [42] Peter, J., De Chiara, M., Friedrich, A., Yue, J. X., Pflieger, D., Bergström, A., Sigwalt, A., Barre,  
524 B., Freel, K., Llored, A., Cruaud, C., Labadie, K., Aury, J. M., Istace, B., Lebrigand, K., Barbry,

- P., Engelen, S., Lemainque, A., Wincker, P., Liti, G. and Schacherer, J. 2018, ‘Genome evolution across 1,011 *Saccharomyces cerevisiae* isolates’, *Nature* **556**(7701), 339–344.
- 514
- [43] Ram, Y., Dellus-Gur, E., Bibi, M., Karkare, K., Obolski, U., Feldman, M. W., Cooper, T. F.,  
516 Berman, J. and Hadany, L. 2019, ‘Predicting microbial growth in a mixed culture from growth curve data’, *Proceedings of the National Academy of Sciences* **116**(29), 14698–14707.
- 518 [44] Rancati, G., Pavelka, N., Fleharty, B., Noll, A., Trimble, R., Walton, K., Perera, A., Staehling-Hampton, K., Seidel, C. W. and Li, R. 2008, ‘Aneuploidy underlies rapid adaptive evolution of yeast cells deprived of a conserved cytokinesis motor’, *Cell* **135**(5), 879–893.
- 520
- [45] Robbins, N., Caplan, T. and Cowen, L. E. 2017, ‘Molecular evolution of antifungal drug resistance’, *Annu. Rev. Microbiol.* **71**(1), 753–775.
- 522
- [46] Robinson, D., Vanacloig-Pedros, E., Cai, R., Place, M., Hose, J. and Gasch, A. P. 2023, ‘Gene-by-environment interactions influence the fitness cost of gene copy-number variation in yeast’, *bioRxiv*.
- 524
- 526 [47] Rodrigues, M. L. and Albuquerque, P. C. 2018, ‘Searching for a change: The need for increased support for public health and research on fungal diseases’, *PLoS Negl. Trop. Dis.* **12**(6), 1–5.
- 528 [48] Rutledge, S. D., Douglas, T. A., Nicholson, J. M., Vila-Casadesús, M., Kantzler, C. L., Wangsa,  
530 D., Barroso-Vilares, M., Kale, S. D., Logarinho, E. and Cimini, D. 2016, ‘Selective advantage of trisomic human cells cultured in non-standard conditions’, *Scientific Reports* **6**(June 2015), 1–12.
- 532
- [49] Santaguida, S. and Amon, A. 2015, ‘Short- and long-term effects of chromosome mis-segregation and aneuploidy’, *Nat. Rev. Mol. Cell Biol.* **16**(8), 473–485.
- 534
- [50] Santaguida, S., Vasile, E., White, E. and Amon, A. 2015, ‘Aneuploidy-induced cellular stresses limit autophagic degradation’, *Genes Dev.* **29**(19), 2010–2021.
- 536
- [51] Schvartzman, J. M., Sotillo, R. and Benezra, R. 2010, ‘Mitotic chromosomal instability and cancer: Mouse modelling of the human disease’, *Nat. Rev. Cancer* **10**(2), 102–115.
- 538
- [52] Selmecki, A. M., Dulmage, K., Cowen, L. E., Anderson, J. B. and Berman, J. 2009, ‘Acquisition of aneuploidy provides increased fitness during the evolution of antifungal drug resistance’, *PLoS Genet.* **5**(10), e1000705.
- 540 [53] Selmecki, A. M., Forche, A. and Berman, J. 2010, ‘Genomic plasticity of the human fungal pathogen *Candida albicans*’, *Eukaryot. Cell* **9**(7), 991–1008.

- 542 [54] Selmecki, A. M., Gerami-Nejad, M., Paulson, C., Forche, A. and Berman, J. 2008, ‘An isochromosome confers drug resistance in vivo by amplification of two genes, erg11 and tac1’, *Mol.*  
544 *Microbiol.* **68**(3), 624–641.
- 546 [55] Sheltzer, J. M. and Amon, A. 2011, ‘The aneuploidy paradox: Costs and benefits of an incorrect  
karyotype’, *Trends Genet.* **27**(11), 446–453.
- 548 [56] Sheltzer, J. M., Blank, H. M., Pfau, S. J., Tange, Y., George, B. M., Humpton, T. J., Brito, I. L.,  
Hiraoka, Y., Niwa, O. and Amon, A. 2011, ‘Aneuploidy drives genomic instability in yeast’,  
*Science* **333**(6045), 1026–1030.
- 550 [57] Sheltzer, J. M., Ko, J. H., Replogle, J. M., Habibe Burgos, N. C., Chung, E. S., Meehl, C. M.,  
Sayles, N. M., Passerini, V., Storchova, Z. and Amon, A. 2017, ‘Single-chromosome gains  
552 commonly function as tumor suppressors’, *Cancer Cell* **31**(2), 240–255.
- 554 [58] Sionov, E., Lee, H., Chang, Y. C. and Kwon-Chung, K. J. 2010, ‘*Cryptococcus neoformans*  
overcomes stress of azole drugs by formation of disomy in specific multiple chromosomes’,  
*PLoS Pathog.* **6**(4), e1000848.
- 556 [59] Sisson, S. A., Fan, Y. and Tanaka, M. M. 2007, ‘Sequential monte carlo without likelihoods’,  
*Proceedings of the National Academy of Sciences* **104**(6), 1760–1765.
- 558 [60] Sonti, R. V. and Roth, J. R. 1989, ‘Role of gene duplications in the adaptation of *Salmonella*  
*typhimurium* to growth on limiting carbon sources.’, *Genetics* **123**(1), 19–28.
- 560 [61] Syga, S., David-Rus, D., Schälte, Y., Hatzikirou, H. and Deutsch, A. 2021, ‘Inferring the effect  
of interventions on covid-19 transmission networks’, *Scientific Reports* **11**(1), 1–11.
- 562 [62] Todd, R. T., Forche, A. and Selmecki, A. M. 2017, ‘Ploidy variation in fungi: Polyploidy,  
aneuploidy, and genome evolution’, *Microbiol. Spectr.* **5**(4), 1–20.
- 564 [63] Toni, T., Welch, D., Strelkowa, N., Ipsen, A. and Stumpf, M. P. 2009, ‘Approximate bayesian  
computation scheme for parameter inference and model selection in dynamical systems’, *J. R.  
566 Soc. Interface* **6**(31), 187–202.
- 568 [64] Torres, E. M., Dephoure, N., Panneerselvam, A., Tucker, C. M., Whittaker, C. A., Gygi, S. P.,  
Dunham, M. J. and Amon, A. 2010, ‘Identification of aneuploidy-tolerating mutations’, *Cell*  
**143**(1), 71–83.
- 570 [65] Torres, E. M., Sokolsky, T., Tucker, C. M., Chan, L. Y., Boselli, M., Dunham, M. J. and Amon,

- A. 2007, ‘Effects of aneuploidy on cellular physiology and cell division in haploid yeast’, *Science* 572 (80-). **317**(5840), 916–924.
- [66] Tsai, H. J., Nelliat, A. R., Choudhury, M. I., Kucharavy, A., Bradford, W. D., Cook, M. E., Kim, 574 J., Mair, D. B., Sun, S. X., Schatz, M. C. and Li, R. 2019, ‘Hypo-osmotic-like stress underlies general cellular defects of aneuploidy’, *Nature* .
- 576 [67] Williams, B. R., Prabhu, V. R., Hunter, K. E., Glazier, C. M., Whittaker, C. a., Housman, D. E. and Amon, A. 2008, ‘Aneuploidy affects proliferation and spontaneous immortalization in 578 mammalian cells’, *Science* **322**(5902), 703–709.
- 580 [68] Yang, F., Todd, R. T., Selmecki, A., Jiang, Y. Y., Cao, Y. B. and Berman, J. 2021, ‘The fitness costs and benefits of trisomy of each *Candida albicans* chromosome’, *Genetics* **218**(2), 1–7.
- 582 [69] Yona, A. H., Frumkin, I. and Pilpel, Y. 2015, ‘A relay race on the evolutionary adaptation spectrum’, *Cell* **163**(3), 549–559.
- 584 [70] Yona, A. H., Manor, Y. S., Herbst, R. H., Romano, G. H., Mitchell, A., Kupiec, M., Pilpel, Y. and Dahan, O. 2012, ‘Chromosomal duplication is a transient evolutionary solution to stress.’, *Proceedings of the National Academy of Sciences* **109**(51), 21010–5.
- 586 [71] Zhu, J., Pavelka, N., Bradford, W. D., Rancati, G. and Li, R. 2012, ‘Karyotypic determinants of chromosome instability in aneuploid budding yeast’, *PLoS Genetics* **8**(5).
- 588 [72] Zhu, J., Tsai, H.-J., Gordon, M. R. and Li, R. 2018, ‘Cellular stress associated with aneuploidy’, *Dev. Cell* **44**(4), 420–431.
- 590 [73] Zhu, Y. O., Sherlock, G. and Petrov, D. A. 2016, ‘Whole genome analysis of 132 clinical *Sac- 592 charomyces cerevisiae* strains reveals extensive ploidy variation’, *G3 Genes, Genomes, Genetics* **6**(8), 2421–2434.
- 594 [74] Zhu, Y. O., Siegal, M. L., Hall, D. W. and Petrov, D. A. 2014, ‘Precise estimates of mutation rate and spectrum in yeast’, *Proceedings of the National Academy of Sciences* **111**(22), E2310–E2318.

# Supplementary Material

## 596 Supplementary Analysis

**Sensitivity analysis.** Changing a single parameter while keeping the rest fixed at the MAP estimate produces a worse fit to the data (Figure S6). Furthermore, we fitted models with a mutation rate fixed at  $\mu = 10^{-5}$ ,  $10^{-6}$  and  $10^{-7}$ . We inferred similar parameters estimates for the model with  $\mu = 10^{-6}$  compared to the model with a free  $\mu$  parameter, in which the inferred mutation rate is  $\mu \approx 3 \cdot 10^{-6}$ . Inference assuming  $\mu = 10^{-5}$  or  $\mu = 10^{-7}$  produced similar estimates except that the estimated aneuploidy rate,  $\delta$ , was higher, and assuming  $\mu = 10^{-7}$ , the estimated fitness of  $2n+1$  was lower (Figure S7).

**604 Extended informative prior distribution.** In an extended informative prior distribution, we used additional growth curves of  $2n^*$  (*refined* strain from Yona et al.<sup>70</sup>) and  $2n+1$  in 39 °C to estimate  $w_{2n^*}/w_{2n+1}$  (Figure S3L). The same distribution was used for  $w_{2n^*}/w_{2n+1*}$ . Thus, our main informative prior uses a single prior distribution for fitness values of  $2n+1$ ,  $2n+1^*$ , and  $2n^*$ , whereas the extended informative prior uses one distribution for  $2n+1$ , and another distribution for both  $2n+1^*$  and  $2n^*$ .

We estimated the parameters under this extended informative prior. Inference took much longer to run but the posterior distribution seemed to converge, as it did not change much in the final iterations. The posterior predictive plot shows that inference with this extended prior produces a posterior distribution that fails to explain the empirical observations (pink in Figure 3). However, the inferred posterior distribution is considerably narrower (compare Figures 2 and S8) and therefore parameter estimates are less variable. The estimated mutation rate was much lower compared to the main informative prior, with  $\mu = 2.474 \cdot 10^{-9}$  [ $2.423 \cdot 10^{-9} - 2.612 \cdot 10^{-9}$ ]. Other parameter estimates are:  $\delta = 2.705 \cdot 10^{-3}$  [ $2.094 \cdot 10^{-3} - 3.094 \cdot 10^{-3}$ ],  $w_{2n+1} = 1.022$  [ $1.021 - 1.024$ ],  $w_{2n+1^*} = 1.052$  [ $1.05 - 1.054$ ],  $w_{2n^*} = 1.053$  [ $1.051 - 1.055$ ], the latter two being much higher compare to the main informative prior. Notably, the mode of the posterior ratio  $w_{2n^*}/w_{2n+1} = 1.0009$  is much lower than the mode of the prior ratio of 1.033 (Figure S3H) and closer to the ratio of 1 that we assume in the main informative prior. Together with the posterior predictive results, we conclude that the main informative prior is preferable over the extended informative prior.

**Model with transitions to less-fit genotypes** We also estimated the parameters of a version of the model that includes transitions (mutation, chromosome loss and gain) to less-fit genotypes (e.g.,  $2n^*$

to  $2n+1^*$ ),

$$\begin{aligned}
 f_{2n}^m &= (1 - \delta - \mu)f_{2n}^s + \delta f_{2n+1}^s + \mu f_{2n^*}^s , \\
 f_{2n+1}^m &= \delta f_{2n}^s + (1 - \delta - \mu)f_{2n+1}^s + \mu f_{2n+1^*}^s , \\
 f_{2n+1^*}^m &= \mu f_{2n+1}^s + (1 - \delta - \mu)f_{2n+1^*}^s + \delta f_{2n^*}^s , \\
 f_{2n^*}^m &= \mu f_{2n}^s + \delta f_{2n+1^*}^s + (1 - \delta - \mu)f_{2n^*}^s .
 \end{aligned} \tag{7}$$

The inferred values are slightly different. The estimated mutation rate,  $\mu = 1.036 \cdot 10^{-7}$  [8.01 · 628  $10^{-8} - 1.339 \cdot 10^{-7}$ ], corresponds to a mutation target size of  $\sim 300 - 500$ , assuming the mutation rate per base pair is roughly  $2 \cdot 10^{-10}$  (ref.<sup>74</sup>) or  $3.3 \cdot 10^{-10}$  (ref.<sup>35</sup>). The estimated aneuploidy 630 rate,  $\delta = 2.358 \cdot 10^{-4}$  [ $1.766 \cdot 10^{-4} - 2.837 \cdot 10^{-4}$ ] is 5-35-fold higher than in previous studies: 632 for Chromosome III in diploid *S. cerevisiae*, Zhu et al.<sup>74</sup> estimated  $6.7 \cdot 10^{-6}$  chromosome gain 634 events per generation, and Kumaran et al.<sup>32</sup> estimate  $3.0 - 4.3 \cdot 10^{-5}$  chromosome loss events per 636 generation (95% confidence interval). The estimated fitness values are  $w_{2n+1} = 1.024$  [1.023 – 1.025], 638  $w_{2n+1^*} = 1.025$  [1.024 – 1.026],  $w_{2n^*} = 1.032$  [1.031 – 1.033], all relative to the fitness of  $2n$ , which 640 is set to  $w_{2n} = 1$ . Thus, we can infer that the cost of trisomy is  $c = w_{2n^*} - w_{2n+1^*} = 0.007$  (or 0.7%) 642 and the benefit of trisomy is  $w_{2n+1} - 1 - c = 0.017$  (1.7%), whereas the benefit of beneficial mutation is  $w_{2n^*} - 1 = 0.032$  (3.2%).

638 We simulated genotype frequency dynamics using parameter samples from the posterior distribution, 640 and computed the posterior distribution of  $F_A$ . The mean  $F_A$  in this case is just 0.0189 [0.0004 - 642 0.1214 95% CI], lower than without the transitions to less-fit genotypes. Here,  $F_A$  is the sum of frequencies of both  $2n_A^*$  and  $2n + 1_A^*$ , which reaches a frequency of 0.0007. Out of 100,000 posterior samples, none had  $F_A$  above 0.05 (i.e., 5% of the population).

## Supplementary Figures & Tables

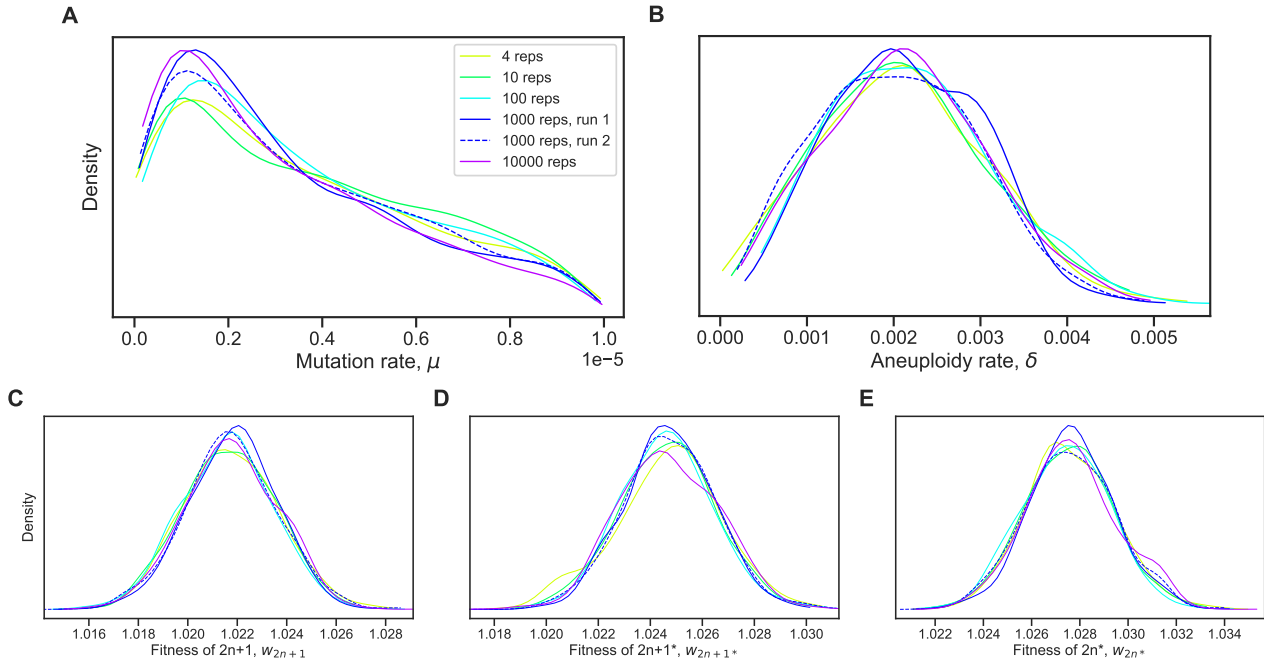


**Figure S1: Posterior distribution validation.** The posterior distribution of model parameters is roughly the same regardless of the number of simulations (4-10,000 replicates) used to approximate the likelihood (eq. (4)).

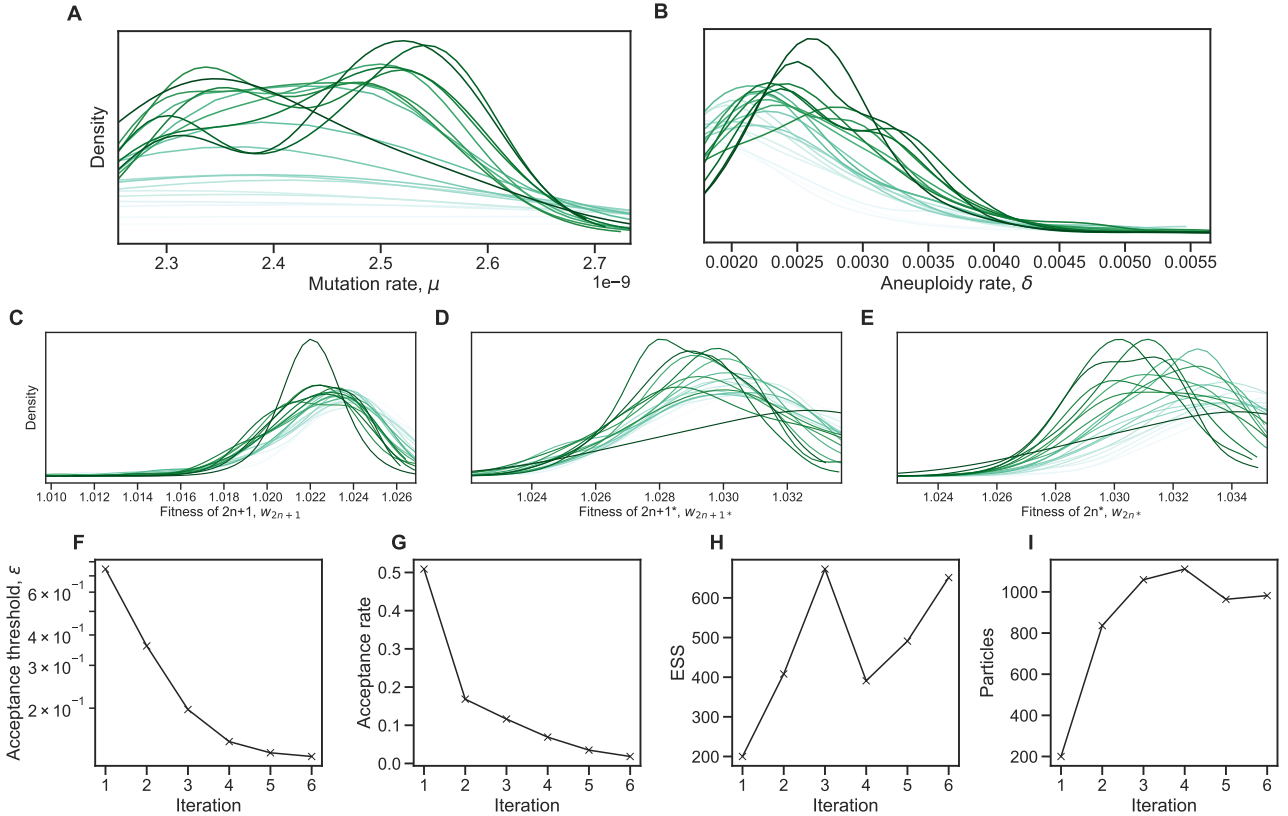


**Figure S2: Inference convergence.** The ABC-SMC algorithm was used to infer the model parameters. **(A-E)** The approximate posterior distributions of model parameters at each iteration of the ABC-SMC algorithm demonstrates convergence, as the posterior did not significantly change after the first iteration,  $t = 1$ . **(F-I)** ABC-SMC measures of convergence. After iteration number 6, the acceptance threshold was  $\epsilon = 0.13$  (i.e.,  $\mathcal{L} = 0.87$ , eq. (4)), the acceptance rate was 0.018, the number of particles was 982, and the effective sample size ESS=651.

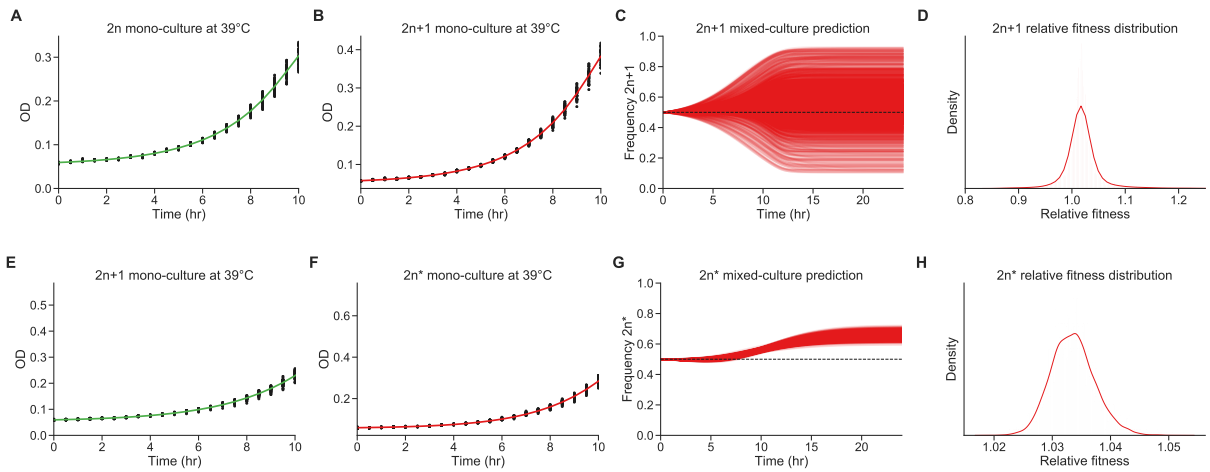


**Figure S3: Fitness estimation from growth curves.** **(A-D)** Fitness estimation from growth curves of  $2n$  and  $2n+1$  at  $39^{\circ}\text{C}$ .  $w_{2n+1}/w_{2n}=1.024$  (95% CI: 0.959 - 1.115). **Curveball (E-H)** Fitness estimation from growth curves of  $2n+1$  and  $2n^*$  at  $39^{\circ}\text{C}$ .  $w_{2n^*}/w_{2n+1}=1.033$  (95% CI: 1.027 - 1.041). Growth curves previously described in Yona et al.<sup>70</sup>, Figs. 3C, 4A, and S2. Fitness estimated from growth curves using Curveball, a method for predicting results of competition experiments from growth curve data<sup>43</sup> [curveball.yoavram.com](http://curveball.yoavram.com). See *Models and Methods, Prior distributions* for more details. **(A,B;E,F)** Mono-culture growth curve data (markers) and best-fit growth models (lines). **(C,G)** The mixed-culture prediction for the strains from A,B and E,F respectively, 6,375 generated curves. **(D,H)** The relative fitness distribution for  $2n+1$  relative to  $2n$  (panel D) and  $2n^*$  relative to  $2n+1$  (panel H). Figures generated by Curveball.

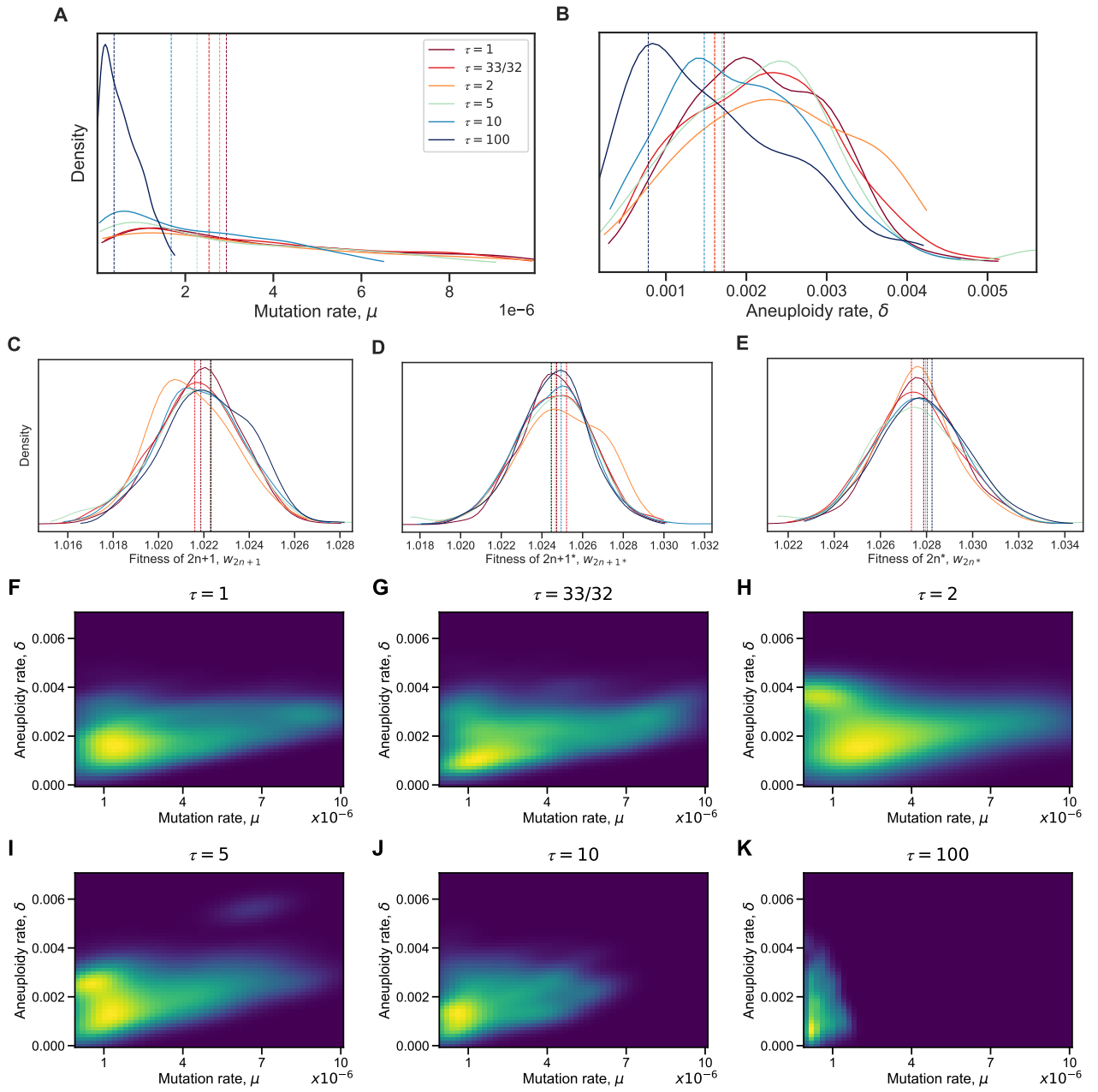


**Figure S4: Model with elevated mutation rate in aneuploid cells.** (A-E) The inferred posterior distributions for models with different values of  $\tau$ , the fold-increase in mutation rate in aneuploid cells ( $2n+1$  and  $2n+1^*$ ). Vertical dashed lines represent the MAP (maximum a posteriori) of each distribution. When the increase in mutation rate is high,  $\tau = 10$  and  $\tau = 100$ , the inferred mutation (A) and aneuploidy (B) rates tend to be lower. (F-K) The inferred joint posterior distribution of mutation rate ( $\mu$ ) and aneuploidy rate ( $\delta$ ) with different  $\tau$  values (dark purple and bright yellow for low and high density, respectively).

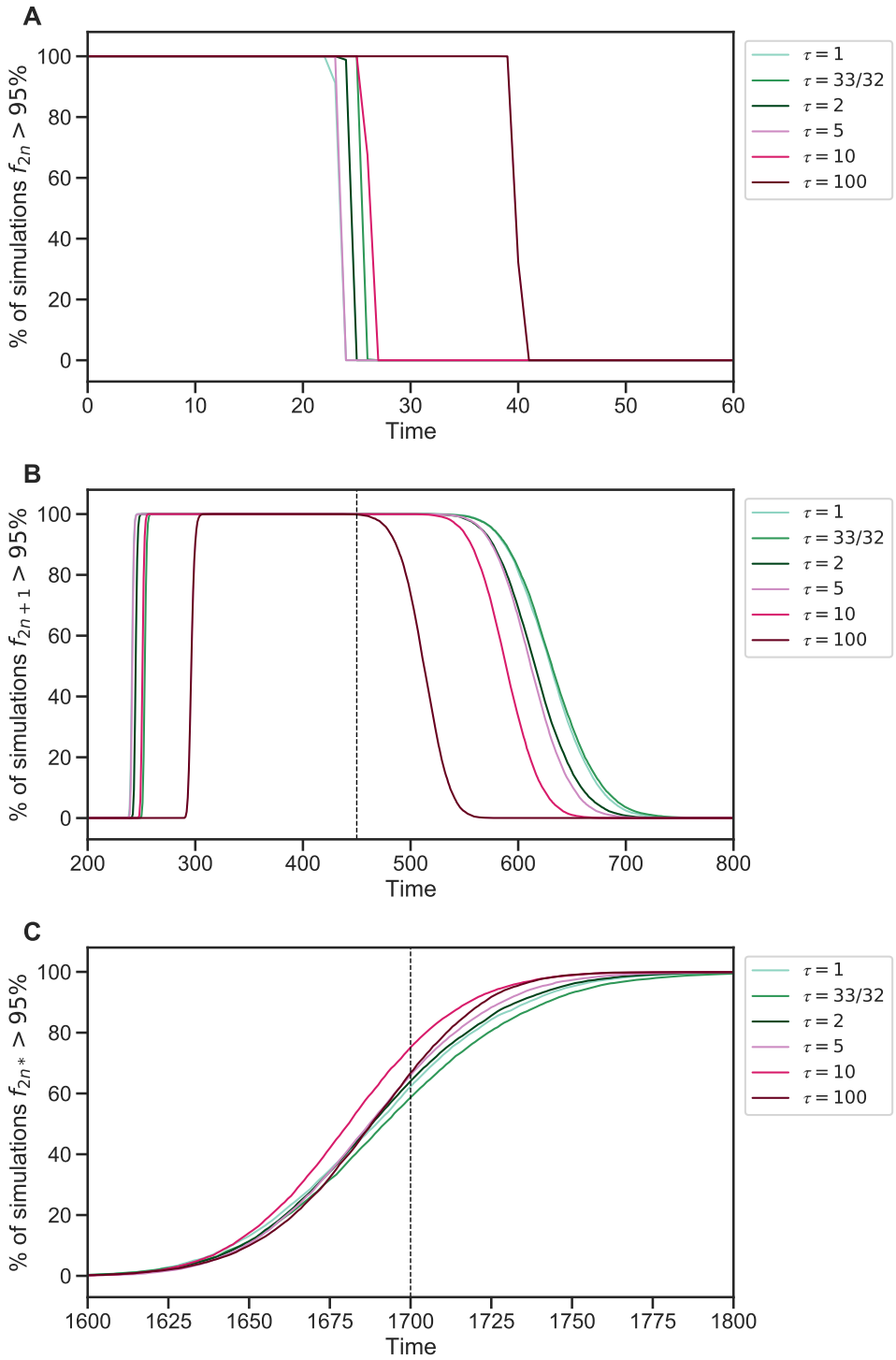


**Figure S5: Genotype fixations for models with increased genetic instability.** We estimated the parameters for different models, each assuming a different value of  $\tau$ , the fold-increase in mutation rate in aneuploid cells. We then generated 10,000 simulations using the MAP estimate of each model and evaluated the fraction of simulations in which the frequency of genotype  $2n$  (**A**),  $2n+1$  (**B**), and  $2n^*$  (**C**) is above 95% (y-axis) at each generation (x-axis). Note that  $2n+1^*$  did not fix. We can see that  $\tau = 100$  can be distinguished if the waiting time for  $f_{2n} < 95\%$  is known (panel A) or if the waiting time for  $f_{2n+1} > 95\%$  or  $f_{2n+1} < 95\%$  is known (panel B). It is harder to distinguish between  $1 \leq \tau \leq 10$ .

**Table S1: WAIC values for different  $\tau$  values.** Differences of less than 6 are considered of weak significance<sup>26</sup>.

Model	WAIC
$\tau = 1$	-9
$\tau = 33/32$	-9
$\tau = 2$	-8
$\tau = 5$	-12
$\tau = 10$	-9
$\tau = 100$	-12

WAIC defined in eq. (6).

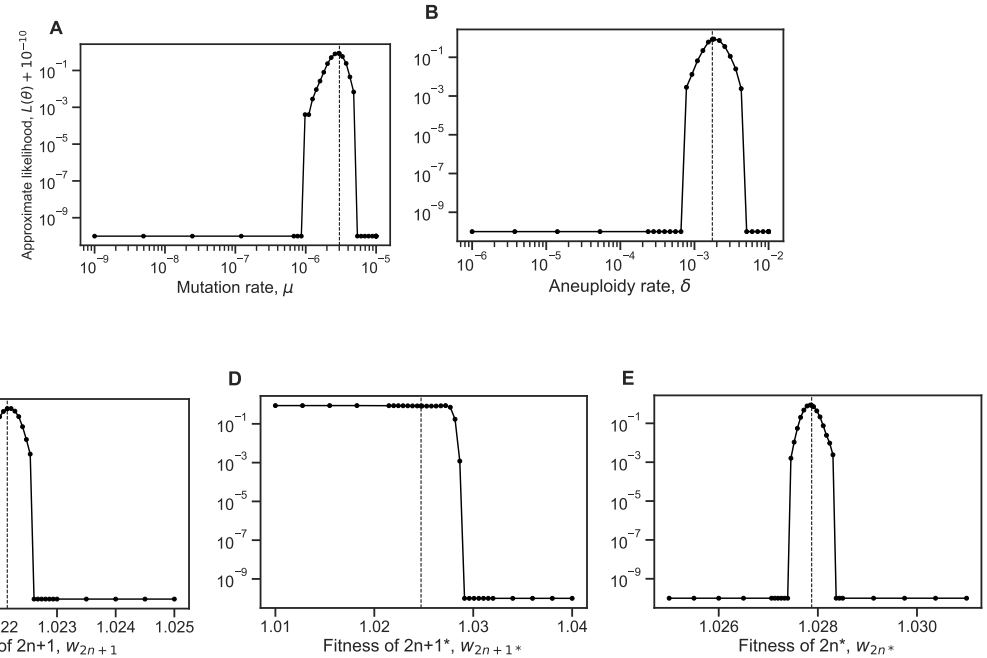


**Figure S6: Likelihood profiles.** Sensitivity of the model approximate likelihood,  $\mathcal{L}(\theta)$ , to changing a single parameter while the other parameters remain fixed at their MAP estimates. Dashed vertical line represents the MAP value. The prior distributions for the mutation rate and aneuploidy rate are  $\mu \sim U(10^{-9}, 10^{-5})$  and  $\delta \sim U(10^{-6}, 10^{-2})$ , respectively.

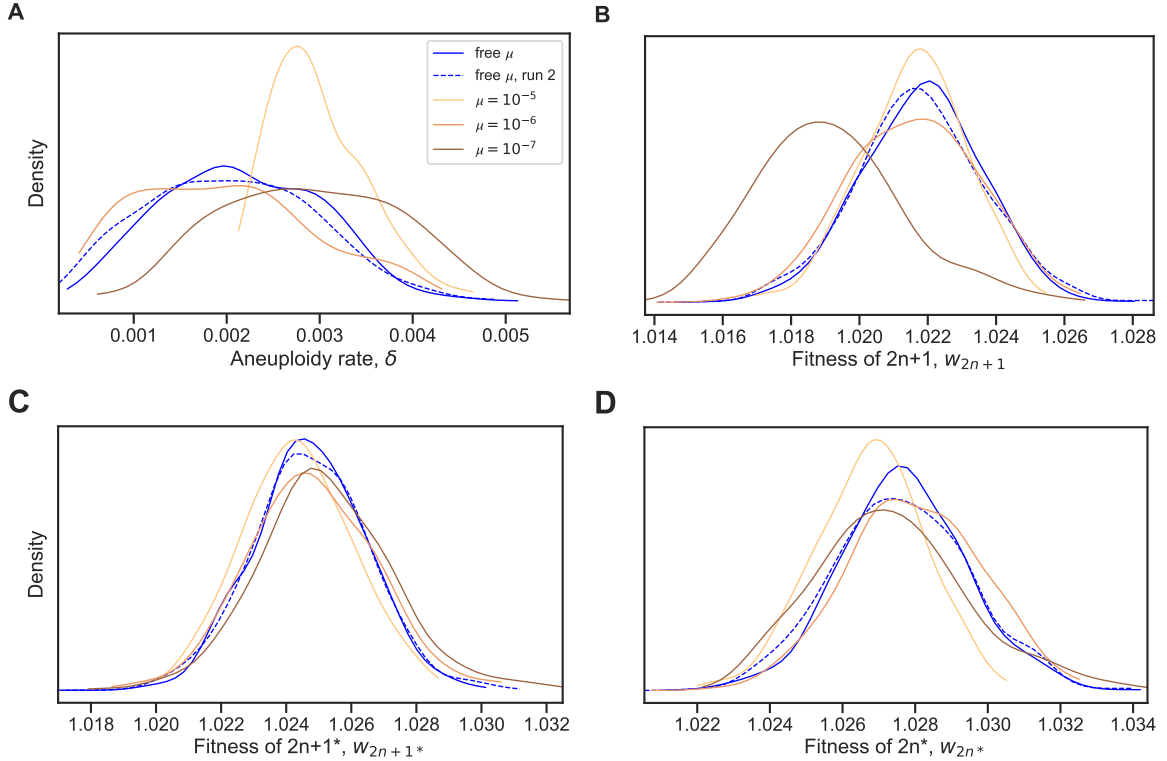


**Figure S7: Model with fixed mutation rate.** (A-D) The inferred posterior distributions for models with free and fixed mutation rate,  $\mu$ . The MAP (maximum a posteriori) and 50% HDI (highest density interval) for each model are: **free  $\mu$ , run 1:**  $\delta = 1.720 \cdot 10^{-3}$  [ $1.470 \cdot 10^{-3} - 2.786 \cdot 10^{-3}$ ],  $w_{2n+1} = 1.022$  [1.021 – 1.023],  $w_{2n+1^*} = 1.025$  [1.024 – 1.026],  $w_{2n^*} = 1.028$  [1.026 – 1.029]; **free  $\mu$ , run 2:**  $\delta = 2.129 \cdot 10^{-3}$  [ $1.334 \cdot 10^{-3} - 2.695 \cdot 10^{-3}$ ],  $w_{2n+1} = 1.022$  [1.02 – 1.023],  $w_{2n+1^*} = 1.025$  [1.023 – 1.026],  $w_{2n^*} = 1.028$  [1.026 – 1.029];  **$\mu = 10^{-5}$ :**  $\delta = 2.903 \cdot 10^{-3}$  [ $2.399 \cdot 10^{-3} - 3.156 \cdot 10^{-3}$ ],  $w_{2n+1} = 1.022$  [1.021 – 1.023],  $w_{2n+1^*} = 1.024$  [1.023 – 1.025],  $w_{2n^*} = 1.027$  [1.026 – 1.028];  **$\mu = 10^{-6}$ :**  $\delta = 1.917 \cdot 10^{-3}$  [ $9.624 \cdot 10^{-4} - 2.447 \cdot 10^{-3}$ ],  $w_{2n+1} = 1.022$  [1.02 – 1.023],  $w_{2n+1^*} = 1.025$  [1.023 – 1.026],  $w_{2n^*} = 1.028$  [1.027 – 1.029];  **$\mu = 10^{-7}$ :**  $\delta = 2.901 \cdot 10^{-3}$  [ $2.139 \cdot 10^{-3} - 3.671 \cdot 10^{-3}$ ],  $w_{2n+1} = 1.019$  [1.017 – 1.02],  $w_{2n+1^*} = 1.025$  [1.024 – 1.026],  $w_{2n^*} = 1.027$  [1.026 – 1.029].

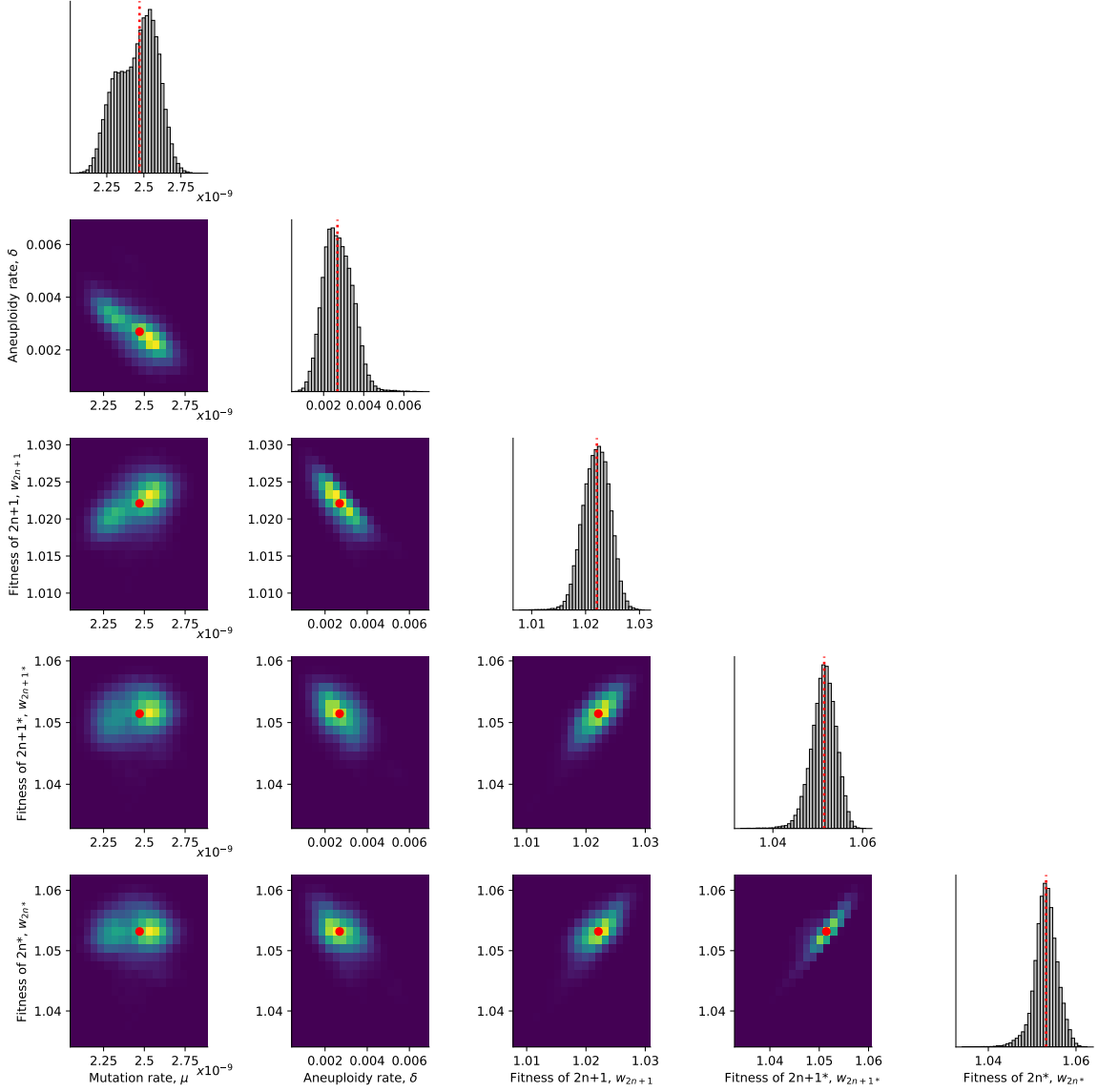


**Figure S8: Posterior distribution of parameters inferred with the extended prior distribution.** On the diagonal, the inferred posterior distribution of each model parameter. Below the diagonal, the inferred joint posterior distribution of pairs of model parameters (dark purple and bright yellow for low and high density, respectively). Red markers and orange lines for the joint MAP estimate (which may differ from the marginal MAP, as the marginal distribution integrates over all other parameters).

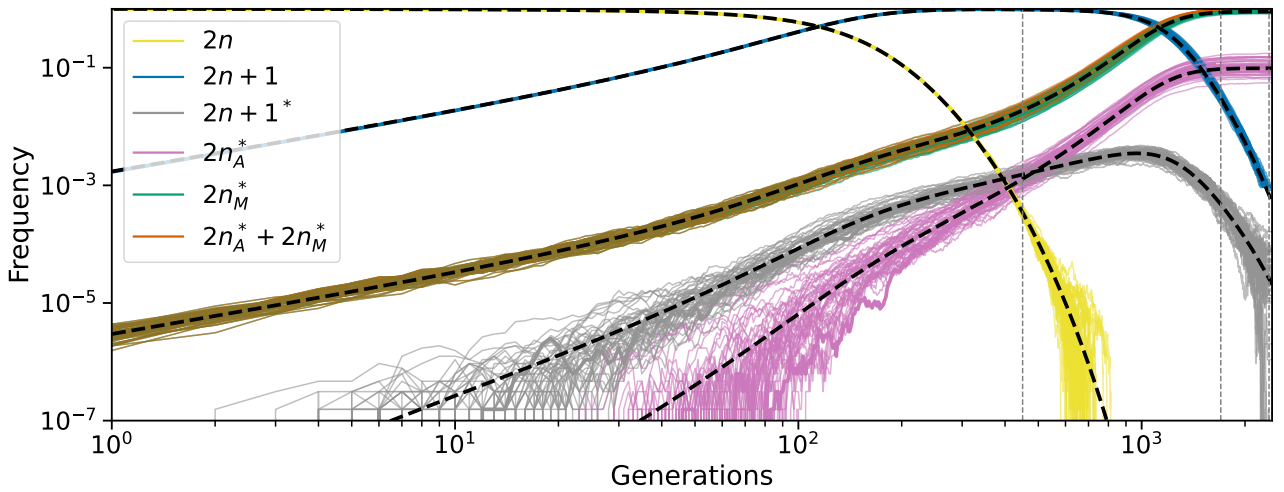


**Figure S9: Posterior predicted genotype frequencies in log-log scale.** Frequency dynamics of the different genotypes with MAP parameter estimates, same as Figure 4A, but in log-log scale. Black dashed curves for a deterministic model without genetic drift. Clearly, appearance of  $2n+1$  and  $2n_M^*$  is deterministic. Appearance of  $2n+1^*$ , and therefore  $2n_A^*$ , is stochastic, however, the frequency dynamics are deterministic above a frequency of roughly 0.001. Note that the  $2n_M^*$  and the  $2n_A^* + 2n_M^*$  lines are overlapping for much of their trajectories.

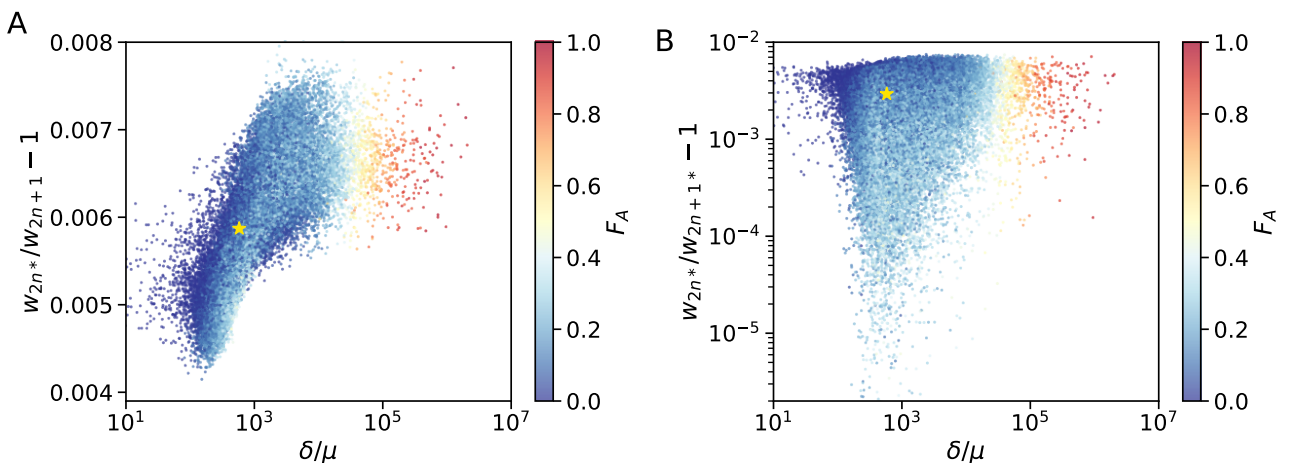


**Figure S10: Posterior distribution of  $F_A$ .** (A,B)  $F_A$  values (color coded) as in Figure 4 for different parameter choices on the x- and y-axes. White star denotes the MAP estimate.